MODULAR MICRO-WIND TURBINE FOR PROVIDING POWER TO TRAIN SENSING SYSTEMS

A Thesis

by

ALEXIS TREVINO

Submitted to the Office of Graduate and Professional Studies of
Texas A&M University
in partial fulfillment of the requirements for the degree of

MASTER OF SCIENCE

Chair of Committee,	Alan Palazzolo
Committee Members,	David Allen
	Won-jong Kim
Head of Department,	Andreas A. Polycarpou

May 2018

Major Subject: Mechanical Engineering

ABSTRACT

The proposed work involves developing a wind turbine system that charges batteries to provide required power of sensing and communication systems, while railroad operates at expected operating conditions. For this project, a 50 mph wind and 50 watts power requirement is assumed. Taking into account inefficiencies and parasitic losses in the wind turbine and electrical system, a blade diameter of 7 inches is calculated to be necessary for this application. Since off the shelf wind turbines are not designed for this specifications, it is necessary to design the most efficient blade shape for this application while also taking into account the electrical charging system power requirements.

For a constant wind speed, a wind turbine blade has a characteristic torque (or power) vs angular velocity curve, that is dependent on the angle of twist and chord length distribution, hub and overall radius, and airfoil of the blade. Similarly, the electrical system has a characteristic torque vs angular velocity (power vs angular velocity) curve that is dependent on the state of charge of the battery. The design approach used in this project was to create several wind turbine blade and electrical system characteristic power curves. Next, the intersection between wind turbine blade and electrical characteristic curve that yields the highest power transfer is used to choose a wind turbine blade shape.

The objective of this work is to develop a battery charging system along with an optimized wind turbine blade that provides the highest power transfer to the battery; manufacture the blade with close dimensional agreement; and test on a wind tunnel to compare theoretical and experimental torque, power, and efficiency curves as well as charging of battery.

ACKNOWLEDGEMENTS

First of all, I would like to thank Dr. Palazzolo for his continuous support, guidance, and technical expertise throughout the project. Thanks to TTI and the Center for Railway Research for funding this project. I would also like to thank to Dr. David Allen and Dr. Won-jong Kim for their time serving as my committee members. A special thanks to Erwin “Tom” Thomas for his help setting up the test rig, testing, and support. Also, thanks to members of the VCEL lab in help provided.

CONTRIBUTORS AND FUNDING SOURCES

Contributors

This work was supported by a thesis committee consisting of Dr. Palazzolo (advisor) and Dr. Kim of the Department of Mechanical Engineering and Dr. Allen of the Department of Civil Engineering.

Funding Sources

This work was made possible in part by the Center for Railway Research (CRR) and Texas A&M Transportation Institute (TTI).

NOMENCLATURE

a Axial interference or induction factor

a’ Angular induction factor

A Projected airfoil area (chord span), surface area, rotor swept area

B Number of blades

BEM Blade Element Momentum

c Airfoil chord length

C_d Two-dimensional drag coefficient

CFM Cubic feet per minute

C_l Two-dimensional lift coefficient

C_L Three-dimensional lift coefficient

C_P Power coefficient

C_T Thrust coefficient or local thrust coefficient

CFD Computational Fluid Dynamics

dA Annular area

dr Thickness

dF_D drag force for blade element

dF_L Lift force for blade element

dF_N Normal force for blade element

dF_T Tangential force for blade element

dQ Torque for blade element; Torque in annular area dA

dT Thrust for blade element; Thrust in annular area dA

FEA Finite Element Analysis

F_D Drag force

F_L Lift force

F_N Normal force, force normal to plane of rotation (thrust)

F_T (i) Force tangential to circle swept by blade section

l length

$\dot{m}$ Mass flow rate

N Number of blade elements

p Pressure

P Power

Q Torque

r Radius

r_h Rotor radius at the hub

r_i Radius at the midpoint of a blade section

R Outer blade radius

SOC State of Charge

T Thrust

U Characteristic velocity, mean air flow velocity

α Angle of attack

λ Tip speed ratio

ρ Air density

σ Rotor solidity

φ Angle of relative wind

ω Angular velocity of the wind

Ω Angular velocity of the wind turbine rotor

θp twist angle, section pitch angle

TABLE OF CONTENTS

Page

LIST OF FIGURES

Page

LIST OF TABLES

Page

1. INTRODUCTION

Use of remote, distributed sensing systems on trains will assist in improving performance and safety. The proposed work involves developing remotely located micro wind turbine generators to charge batteries that power sensing and communications systems. The turbines will be modular packages that are easily attached to any car in the train. Other researchers have harvested energy utilizing the vibration in the suspension to actuate piezo generators. Some tracks are smooth causing little vibration, hence we utilize a more dependable harvested energy source, i.e. train induced windage and draft.

A combined wind turbine generator – solar panel system will be also be developed for track-side units to charge batteries from the natural wind, draft of the train and from the sun. The batteries can power stationary instrumentation for track condition monitoring and other applications. The turbine may be embedded in the track or positioned track side as shown in Figure 1.

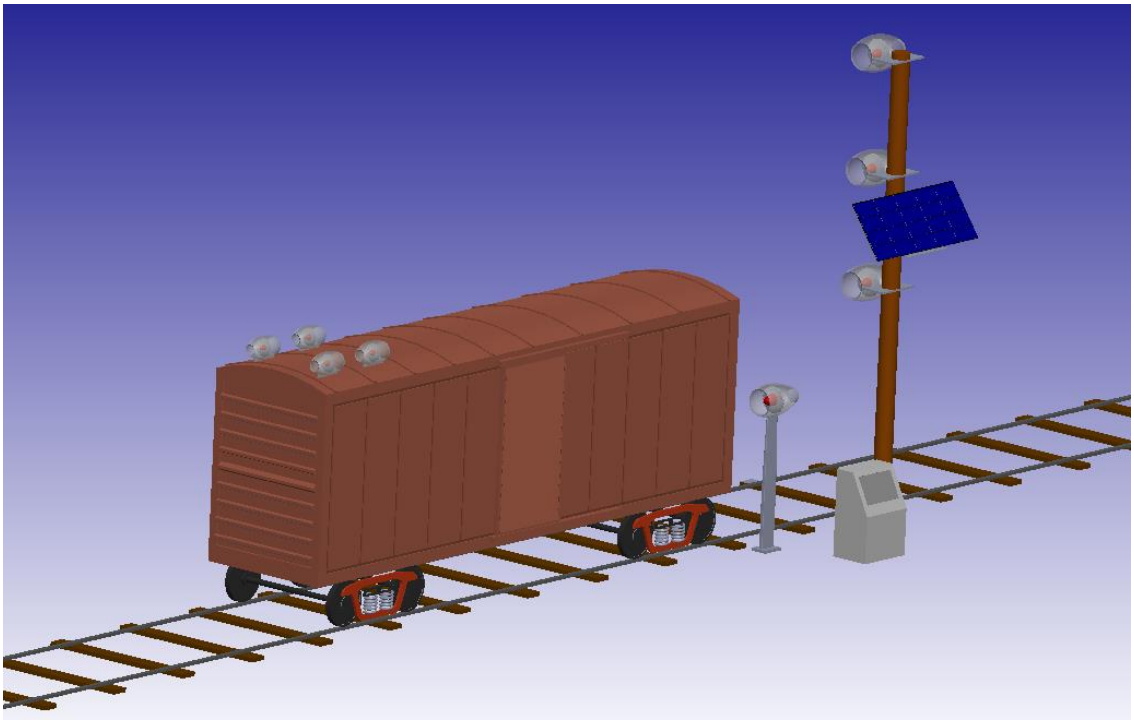

Figure 1-Concept illustration of wind turbines

1.1 Problem statement

Typical train cars travel at 50 mph; therefore, it was initially assumed that a wind turbine on top of a train car would perceive a 50 mph wind derived from the train motion. Also, 50 watts power requirement by typical train sensing systems was decided from the opinion of a railroad expert form the Association of American Railroads (AAR).

The power per square meter of cross section area for a 50 mph (22.3 m/s) wind is 6.4 kW. Betz's law says that at most 59% of this can be harvested (4 kW per meter^2). In practice the efficiency for wind turbine conversion is about 45% (3 kW per meter^2). Converting the wind power to power delivered by batteries involves the additional efficiencies: Generator (80%), Power Inverter (80%) and Battery (90%). This make the power available from the battery about 1700 watts / meter^2. Most sensors require less than 1 watt of power, so 10 sensors will require less than 10 watts of power. In addition the data acquisition and communication budget is estimated at 40 watts max. This sums to about 1/30 of the 1500 watts / meter^2, so the area would need to be 1/30 meter^2 to provide the 50 Watts of battery power. Doubling this amount for surplus power, charging and other parasitic losses yield an area of 1/15 meter^2. Dividing this among 2 wind turbines yields a 1/30 meter^2 flow area requirement for each turbine. This is equivalent to an 18 cm (7 inch) flow diameter.

Blade element momentum theory (BEM) is a theory that combines blade element theory and momentum theory. In the blade element theory, a wind turbine blade is discretized into "blade elements"; forces are calculated on each of the elements at a given wind speed and angular velocity. The blade element theory is combined with momentum theory in order to calculate induction factors; where induction factors are factors used to take into account the reduction in axial velocity and increase in tangential velocity of wind close to the rotor. Through the BEM theory, the optimal twist angles and chord length for each blade element can be optimized to maximize power output of wind turbine.

The harvester system will consist of multiple wind turbine generators, each approximately 7" in diameter by 7" long, with streamlined profiles and attached to the top of a train car. The control and power electronics will be housed in the cylinder. Electrical cables will be routed to the battery packs mounted inside the train car. The batteries will be charged at any wind (train)

speed, and deliver power to the sensors at speed or when the train is stopped. Trackside turbines will be larger to harvest the slower wind speed draft and ambient wind power.

1.2 Approach

The purpose of this research work is to design a modular wind turbine system that transfers most power to the electrical charging system or battery. The approach taken was designing and building: a test rig, a wind turbine system that charges batteries. The test rig would be composed of a wind tunnel with airflow measurement station. The wind turbine charging system is comprised of the wind turbine blade, a three phase generator, electronics to condition AC power to DC and a charging unit that than would be connected to a battery. The charging system would later be tested to check that the battery is being charged by the wind turbine blade at expected wind of 50 mph.

The Beam Element Momentum (BEM) theory is used initially to create designs that maximizes the power output of the wind turbine blade. The commercial software Mecaflux Heliciel applies BEM theory to generate an optimal blade for given conditions. Torque and power vs angular velocity curves are created for several blade curves. Qblade simulation software, which uses BEM theory, is also used to analyze wind turbine blades. Computational Fluid mechanics is used to validate the expected wind velocity perceived by the wind turbines.

Similarly, torque and power vs angular velocity curves are generated experimentally using a motor to drive the electrical system and torque transducer to measure torque. Points of intersection between the blade power curves and electrical system power curves are looked upon to choose an optimal blade design as shown in Figure 2; highest point of power transfer would be looked upon to choose a blade design.

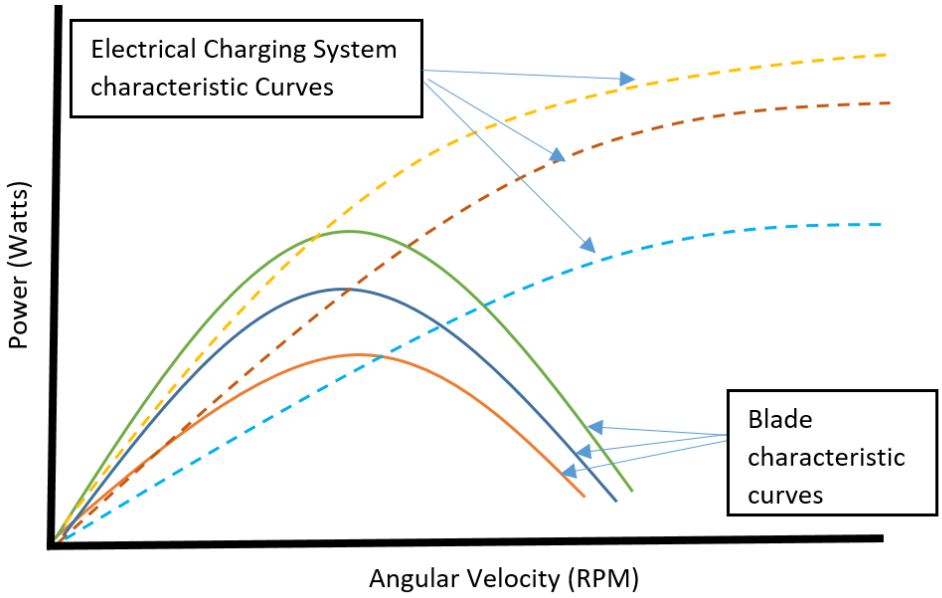

Figure 2-Blade and electrical charging system characteristic curves

Finally, the blade that provides higher power to the electrical charging system is modeled in Solidworks and 3d printed. The blade is then set up with the torque meter into the test rig to validate the blade curves. Torque and power curves are plotted at different angular velocities and compared to BEM torque and power results. Charging of the battery using the optimized wind turbine blade would be then tested.

2. THEORY

2.1 Aerodynamics of wind turbines

In this section, the principles used in the design and optimization of wind turbines are discussed. Like an airplane wing, a wind turbine uses the lift forces produced by wind going through an airfoil element. One difference in the wind turbine is that its airfoil or blade elements perceive an extra component of wind velocity coming from the rotation of the wind turbine. The resultant wind velocity (from incoming and blade rotation) changes along the radius of the blade; therefore it is required to optimize the twist of the blade along its radius to take into account the wind produced by turbine rotation.

A wind turbine blade is composed of several airfoil or blade elements. The wind flow going through the airfoil or blade elements produce forces on the elements that are dependent on the twist angle, chord length and thickness of the blade element. The torque and drag forces on the wind turbine are calculated in each blade element.

First, the one-dimensional (axial) momentum theory and Betz limit is discussed followed by conservation of angular momentum. Afterwards, airfoil theory and blade element theory is introduced. Next, the blade element theory which is used to calculate the performance of a blade design is presented and how it can be used to optimize blade geometry is discussed.

2.1.1 One-dimensional momentum theory and Betz limit

In this section, the conservation of one-dimensional momentum is discussed for a flow going through a steam tube; through this analysis, the maximum theoretical power, or Betz limit, for a wind turbine is obtained.

This analysis assumes a control volume, in which the control volume boundaries are the surface of a stream tube and two cross-sections of the stream tube (see Figure 3). The only flow is across the ends of the stream tube. The turbine is represented by a uniform ‘actuator disc’ which creates a discontinuity of pressure in the stream tube of air flowing through it. Note that this analysis is not limited to any particular type of wind turbine [1],

*Part of the data reported in this chapter is reprinted with permission from *Wind energy explained: theory, design and application*, by Manwell, J. F., McGowan, J. G., & Rogers, A. L.,2011, Chichester: John Wiley & Sons.

This analysis uses the following assumptions:

- homogeneous, incompressible, steady state fluid flow;
- no frictional drag;
- an infinite number of blades;
- uniform thrust over the disc or rotor area;
- a non–rotating wake;
- the static pressure far upstream and far downstream of the rotor is equal to the undisturbed ambient static pressure

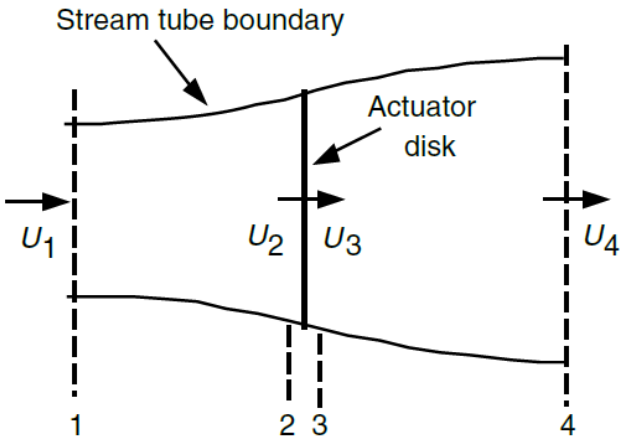

Figure 3-Actuator disc model of a wind turbine; U, mean air velocity; 1, 2, 3, and 4 indicate locations. Reprinted with permission from [1]

Thrust force T on the wind turbine is obtained by applying conservation of linear momentum to the control volume in Figure 3:

$$T = U_1(\rho AU)_1 - U_4(\rho AU)_4 \tag{2.1}$$

For steady flow,$(\rho AU)_{1=}(\rho AU)_4 = \dot{m}$, therefore,

$$T = \dot{m}(U_1 - U_1) \tag{2.2}$$

Since thrust is positive, the velocity behind the rotor U_4 is less than the free stream velocity U_1. We can use Bernoulli's equation in the control volumes on both sides of the actuator disc. For the stream tube upstream of the disc:

$$p_1 + \frac{1}{2}\rho {U_1}^2 = p_2 + \frac{1}{2}\rho {U_2}^2 \tag{2.3}$$

Similarly, in the stream tube downstream of the disc:

$$p_3 + \frac{1}{2}\rho {U_3}^2 = p_4 + \frac{1}{2}\rho {U_4}^2 \tag{2.4}$$

Where it is assumed that the pressures far upstream and far downstream are equal (p_1=p_4) and that the velocity across the disc is the same (U_2=U_3).

We can express the thrust as the net sum of forces on each side of the actuator disc:

$$T = A_2(p_2 - p_3) \tag{2.5}$$

Solving for p_2-p_3 from equations (2.3) and (2.4), assuming that p_1=p_4, U_2=U_3, and substituting into equation (2.5) we get:

$$T = \frac{1}{2}\rho A_2\left({U_1}^2 - {U_4}^2\right) \tag{2.6}$$

Equating thrust equations from Equations (2.2) and (2.6), recognizing that the mass flow rate is $\dot{m} = \rho A_2 U_2$, one obtains:

$$U_2 = \frac{U_1 + U_4}{2} \tag{2.7}$$

Thus, the wind velocity at the rotor plane is the average of the downstream and upstream wind speeds. We define an axial induction factor, a, as the fractional decrease in wind velocity between the free stream and the rotor plane, then

$$a = \frac{U_1 - U_2}{U_1} \tag{2.8}$$

$$U_2 = U_1(1 - a) \tag{2.9}$$

And

$$U_4 = U_1(1 - 2a) \tag{2.10}$$

The power output, P, is equal to the thrust times the velocity at the disc:

$$P = \frac{1}{2}\rho A_2\left({U_1}^2 - {U_4}^2\right)U_2 = \frac{1}{2}\rho A_2 U_2(U_1 + U_4)(U_1 - U_4) \tag{2.11}$$

Substituting the expressions for U2 and U4 shown in equations (2.9) and (2.10), one gets:

$$P = \frac{1}{2}\rho A U^3 4a(1-a)^2 \tag{2.12}$$

Where the control volume area at the rotor, A_2 is replaced by A, the rotor area, and the free stream velocity U_1 is replaced by U.

Wind turbine rotor performance is usually characterized by its power coefficient, C_P:

$$C_P = \frac{P}{\frac{1}{2}\rho U^3 A} = \frac{Rotor\ power}{Power\ in\ the\ wind} \tag{2.13}$$

The non-dimensional power coefficient, CP, represents the fraction of power extracted by the rotor from the available power from wind. Substituting equation (2.12), yields:

$$C_P = 4a(1-a)^2 \tag{2.14}$$

The maximum power coefficient, or Betz limit, is obtained by taking the derivative of equation (2.14) with respect to a and setting it to zero, which yields a=1/3. Thus,

$$C_{P,max} = \frac{16}{27} = 0.5926 \tag{2.15}$$

From equations (2.6), (2.9), and (2.10), the axial thrust on the disc is:

$$T = \frac{1}{2}\rho A U^2 [4a(1-a)] \tag{2.16}$$

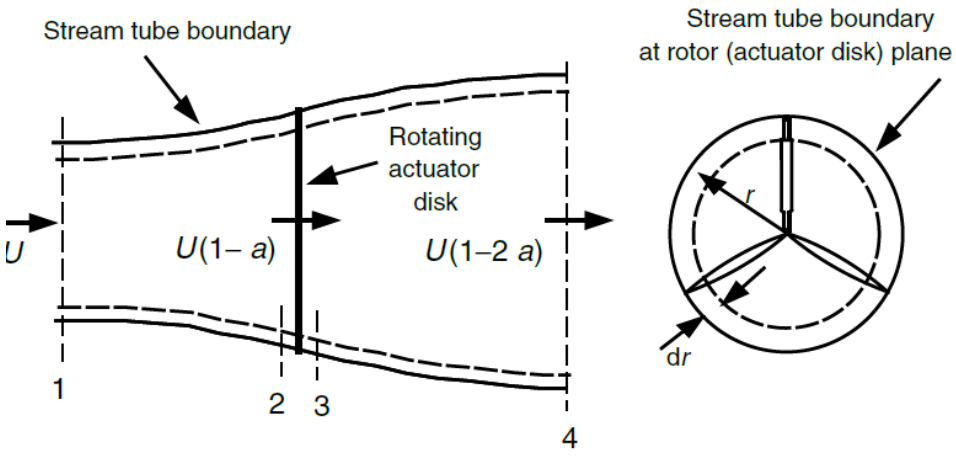

Figure 4-Geometry for rotor analysis; U, velocity of undisturbed air; a, induction factor; r, radius. Reprinted with permission from [1]

One can derive an expression for the torque on the rotor by applying the conservation of angular momentum. For this situation, the torque exerted on the rotor, Q, must equal the change in angular momentum of the wake. On an incremental annular dA=2πrdr area element this gives:

$$dQ = d\dot{m}(\omega r)(r) = (\rho U_2 2\pi r dr)(\omega r)(r) \tag{2.17}$$

Since U_2=U(1-a) and a'=ω/2Ω, this expression reduces to:

$$dQ = 4a'(1-a)\frac{1}{2}\rho U\Omega r^2 2\pi r dr \tag{2.18}$$

2.1.2 Airfoils and general concepts of aerodynamics

Airfoils are structures with specific geometric shapes that are used to generate mechanical forces due to the relative motion of the airfoil and a surrounding fluid. Wind turbine blades use airfoils to develop mechanical power. The cross sections of wind turbines have the shape of airfoils. The width and length of the blade are functions of the desired aerodynamic performance, the maximum desired rotor power, the assumed airfoil properties and strength considerations.

Figure 5 shows an airfoil along with some of the dimensions that define it. In this work, the dimensions that are used are: the angle of attack, and chord. Airflow over an airfoil produces a

lift force, drag force and pitching moment as shown in Figure 6.

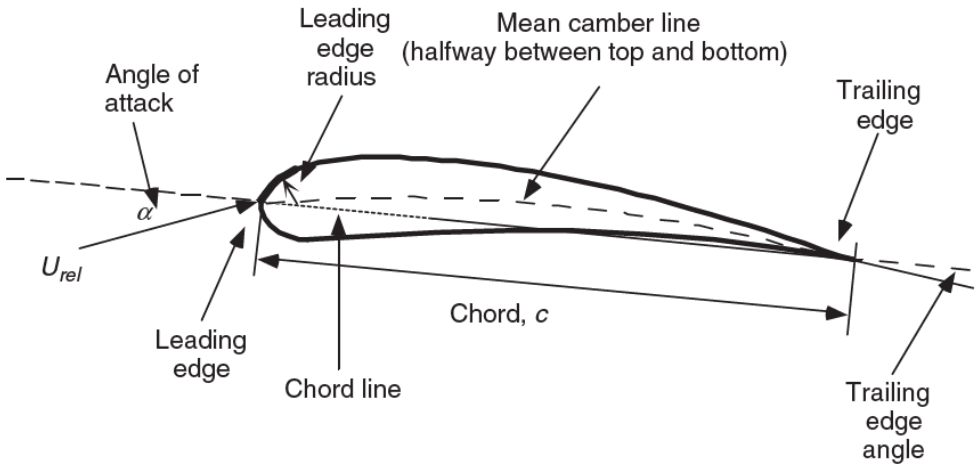

Figure 5-Airfoil nomenclature [1]

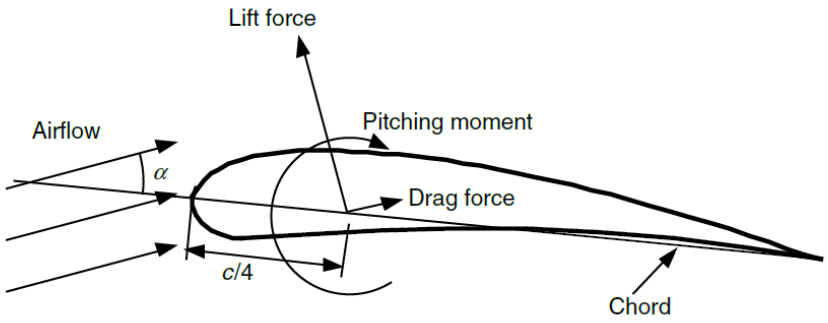

Figure 6-Forces and moments on an airfoil section, α angle of attack; c, chord. Reprinted with permission from [1]

In this work, only lift and drag forces will be looked upon; and can be defined as follows:

$$Lift\ Force = C_l \cdot \frac{1}{2} \cdot \rho \cdot U^2 \cdot c \cdot l \tag{2.19}$$

$$Drag\ Force = C_d \cdot \frac{1}{2} \cdot \rho \cdot U^2 \cdot c \cdot l \tag{2.20}$$

Where Cl and Cd are coefficients that depend on the angle of attack defined in Figure 6, ‘c’ is the chord length of the airfoil, ‘l’ is the length of the airfoil element and U is the wind velocity. Figure 7 shows plots for Cl and Cd versus angle of attack.

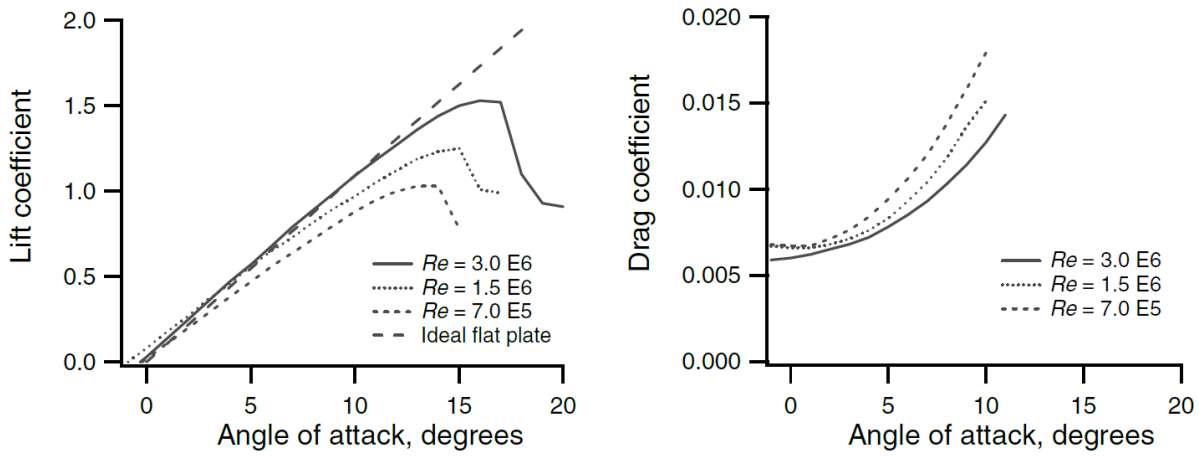

Figure 7-Lift and drag coefficient of NACA 0012 airfoil. Reprinted with permission from [1]

2.1.3 Momentum theory and blade rlement theory

Momentum Theory

Previously we derived the following equations for momentum:

$$dT = \rho U^2 4a(1-a)\pi r dr \tag{2.21}$$

$$dQ = 4a'(1-a)\rho U\pi r^3 \Omega dr \tag{2.22}$$

Blade Element Theory

In the Blade Element Theory, the lift and drag forces produced in an airfoil element will be related to the torque and thrust forces in elements for a wind turbine blade. First, it is important to list the assumptions for the theory.

Assumptions:

-There is no aerodynamic interaction between elements (thus no radial flow)

-The forces on the blades are determined solely by the lift and drag characteristics of the airfoil shape of the blades

It is important to note that a wind turbine blade is composed of several elements as shown in Figure 8. R is the radius of the blade, while r is the distance from the center of the blade. The elements are divided in several elements (usually equal length), for which dr is the length of the element. (For this work, 6 blade elements were used.)

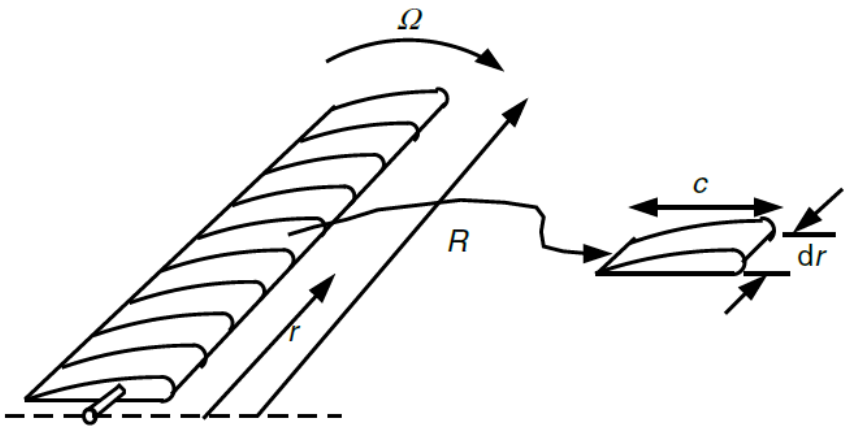

Figure 8-Schematic of blade elements; c, airfoil chord length; dr, radial length of element; r, radius; R, rotor radius; Ω, angular velocity of rotor. Reprinted with permission from [1]

As previously sated, the blade elements perceive an extra component of wind velocity coming from the rotation of the wind turbine. The resultant wind velocity (from incoming and blade rotation) changes along the radius of the blade; therefore it is required to optimize the twist of the blade along its radius to take into account the wind produced by turbine rotation.

Figure 9 shows a cross section of a blade elements along with: the resultant wind velocity composed of incoming wind and blade rotation; lift and drag forces, dF_L and dF_D respectively; and the forces of interest thrust and torque for the blade element, dF_T and dF_N respectively, which can be obtained from lift and drag forces for the blade element, dF_L and dF_D respectively, through geometric approximation related to angle of relative wind ϕ.

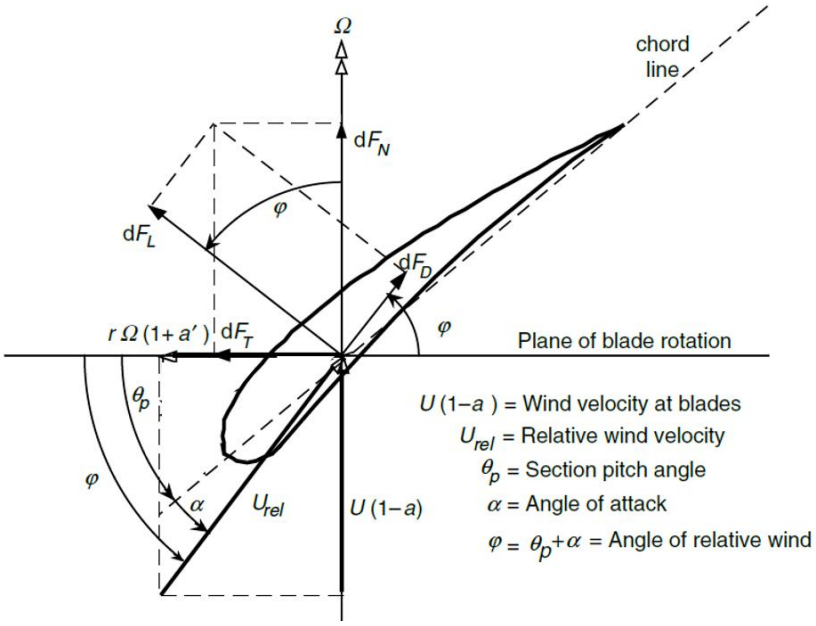

Figure 9-Blade geometry for analysis of a horizontal axis wind turbine. Reprinted with permission from [1]

From Figure 9, on can determine the following relationships, where dF_L and dF_D are lift and drag forces for the blade element:

$$tan\varphi = \frac{U(1-a)}{\Omega r(1+a')} = \frac{1-a}{(1+a')\lambda_r} \tag{2.23}$$

$$U_{rel} = \frac{U(1-a)}{sin\varphi} = \frac{\Omega r(1+a')}{cos\varphi} \tag{2.24}$$

$$dF_L = C_l \frac{1}{2}\rho {U_{rel}}^2 cdr \tag{2.25}$$

$$dF_D = C_d \frac{1}{2}\rho {U_{rel}}^2 cdr \tag{2.26}$$

Calculating the normal and tangential forces for the blade element,

$$dF_N = dF_L cos\varphi + dF_D sin\varphi \tag{2.27}$$

$$dF_T = dF_L sin\varphi - dF_D cos\varphi \tag{2.28}$$

If the blade has B blades, the total normal force on the section at a distance r from the center is:

$$dT = dF_N * B = B\frac{1}{2}\rho {U_{rel}}^2 (C_l cos\varphi + C_d sin\varphi) cdr \tag{2.29}$$

Similarly, the torque for blade element is defined as:

$$dQ = BrdF_T \tag{2.30}$$

$$dQ = B\frac{1}{2}\rho {U_{rel}}^2 (C_l sin\varphi + C_d cos\varphi) crdr \tag{2.31}$$

2.1.4 Blade element momentum

For the previously derived equation for Blade Element Theory, the only missing components, to calculate the torque and drag forces for a wind turbine blade, are the induction factors a and a'. The Blade Element Momentum theory combines the Momentum Theory and Blade Element Theory to get an expression for the inductions factors that are dependent on the blade elements geometry, incoming wind and rotation of the blade. In this section, the expressions for the induction factors a and a' are derived and an algorithm to obtain an optimal blade design is discussed.

Momentum theory

From Momentum theory we obtained the following equations for the thrust dT and torque dQ:

$$dT = \rho U^2 4a(1-a)\pi r dr \tag{2.32}$$

$$dQ = 4a'(1-a)\rho U\pi r^3 \Omega dr \tag{2.33}$$

Blade element theory

Similarly, for the blade element we obtained expressions for thrust dT and torque dQ.

$$dT = dF_N = B\frac{1}{2}\rho {U_{rel}}^2 (C_l cos\varphi + C_d sin\varphi) cdr \tag{2.34}$$

$$dQ = B\frac{1}{2}\rho {U_{rel}}^2 (C_l sin\varphi - C_d cos\varphi) crdr \tag{2.35}$$

Where the relative velocity can be written as a function of the free stream velocity and induction factors, therefore dT and dQ can be written as:

$$dT = \sigma' \pi \rho \frac{U^2(1-a)^2}{sin^2\varphi}(C_l cos\varphi + C_d sin\varphi) r dr \tag{2.36}$$

$$dQ = \sigma' \pi \rho \frac{U^2(1-a)^2}{sin^2\varphi}(C_l sin\varphi - C_d cos\varphi) r^2 dr \tag{2.37}$$

Where σ' is the local solidity, defines as:

$$\sigma' = \frac{Bc}{2\pi r} \tag{2.38}$$

Blade element momentum theory

Equating expressions of torque from momentum and blade element theory we get

$$B\frac{1}{2}\rho {U_{rel}}^2 (C_l cos\varphi + C_d sin\varphi) c dr = \sigma' \pi \rho \frac{U^2(1-a)^2}{sin^2\varphi}(C_l cos\varphi + C_d sin\varphi) dr \tag{2.39}$$

After some algebraic manipulations and solving for the induction factor a, we get, assuming Cd=0:

$$a = \frac{1}{1 + \frac{4sin^2\varphi}{\sigma' C_l cos\varphi}} \tag{2.40}$$

Similarly, equating expressions of normal force from momentum and blade element theory we get:

$$B\frac{1}{2}\rho {U_{rel}}^2 (C_l sin\varphi - C_d cos\varphi) c r dr = \sigma' \pi \rho \frac{U^2(1-a)^2}{sin^2\varphi}(C_l sin\varphi - C_d cos\varphi) r^2 dr \tag{2.41}$$

Solving for a' after some algebraic manipulations reduces to, assuming Cd=0:

$$a' = \frac{1}{\left[\left(\frac{4cos\varphi}{\sigma' C_l}\right) - 1\right]} \tag{2.42}$$

The wind turbine blade optimization then becomes an iterative process. The first step in designing the wind turbine blade starts by defining the rotor diameter, hub diameter, wind speed, angular velocity, number of blade elements, and airfoil of blade elements. For example, 7 inch diameter, 50 mph wind speed, 7000 RPM angular velocity, 5 blade elements and NACA 2411 airfoil.

Next, we can initially assume the induction factors to be zero, assume a value for the blade angle of attack; and use blade element theory to calculate twist angles and chord lengths for each of the blade elements. However, this model will be incorrect because the induction factors, a and a', calculated from equations 2.40 and 2.43 will yield values not equal to zero.

We can than iterate the initial values of the induction factors and repeat the entire process until the assumed induction factors and calculated induction factors are within a close range. Next, the power and the efficiency of the blade can be calculated. If the efficiency is not the desired value, either the chord length or the twist angle, or both can be changed. The entire process is then repeated as shown in the algorithm shown in Figure 10.

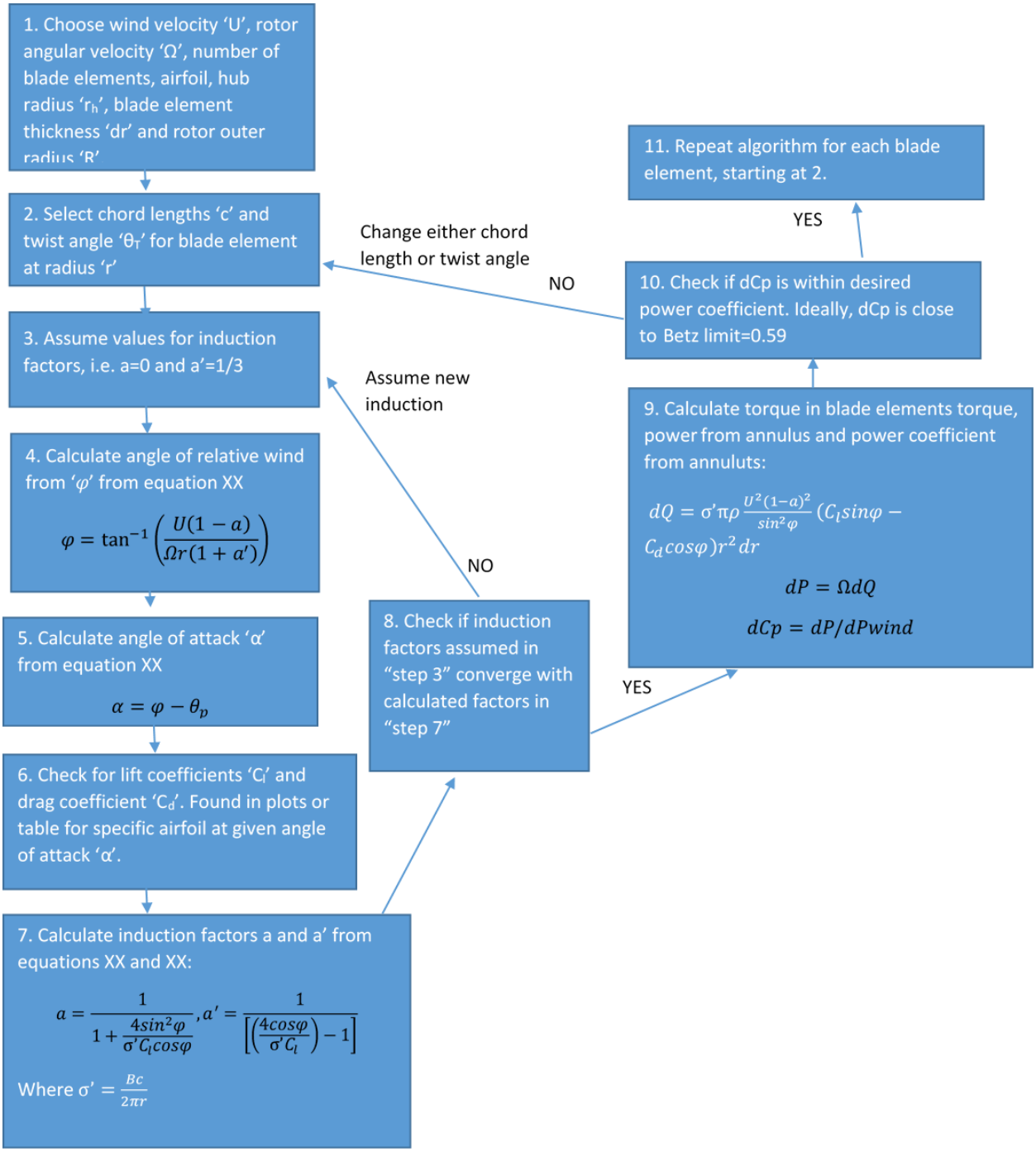

Figure 10-Algorithm for blade elements optimization

If the power coefficient for each element isn't closed to the desire value for step 10, either the chord length or the twist angle can be changed. However, for the wind turbine blade optimization

software Mecaflux Heliciel introduced in section 5.2, a chord length distribution is provided as an input in order to simplify the iteration process. It is useful to provide a chord length distribution since the algorithm might provide a chord length that is not reasonable (chord length cannot be infinite in size). For the work in this project, the chord length distribution was assumed to be constant throughout the radius of the blade. The larger the chord length usually provided higher efficiency for the design optimization using the Mecaflux Heliciel software.

3. TEST RIG AND WIND TURBINE DESIGN

The objective of the design of the test rig was to be able to produce, control and measure the assumed 50 mph wind velocity at a diameter slightly larger than the wind turbine diameter of 7 inches; build a wind turbine fixture that has the ability to measure torque and angular velocity of the wind turbine; and create a charging system that connects from the wind turbine generator to a battery and charges it. Figure 11 and Figure 12 show the final assembly of the test rig. While a detailed explanation of each of the components or systems is discussed in Sections 3.1-3.3. Figure 13 shows a schematic for the charging system.

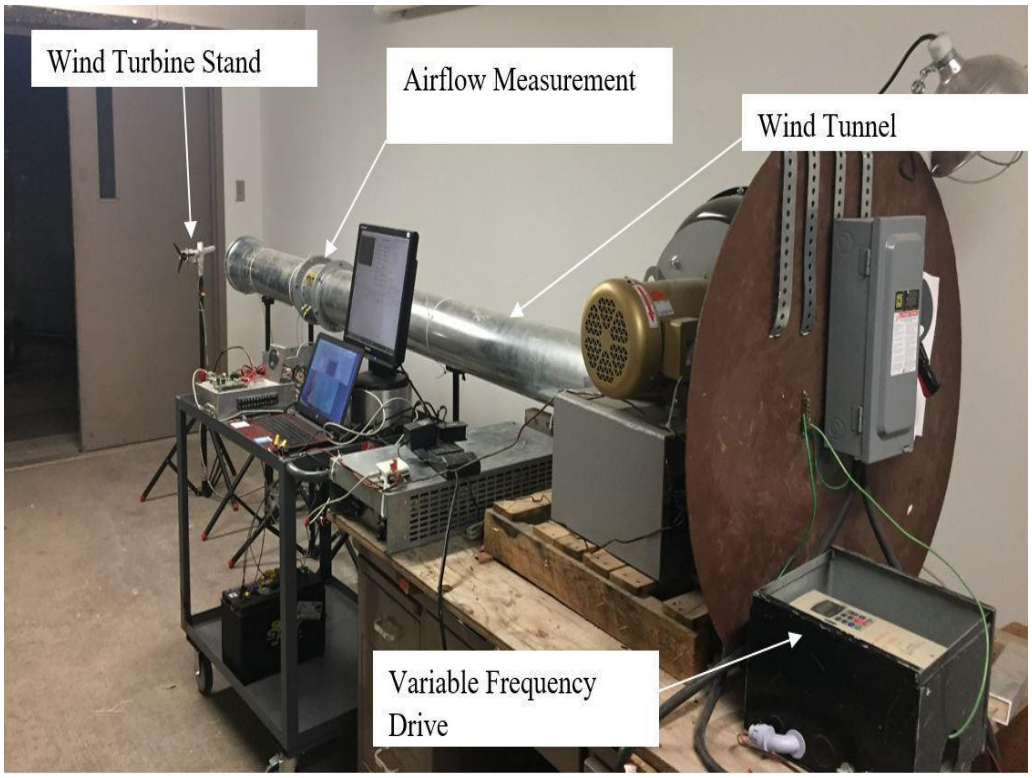

Figure 11-Wind turbine test rig

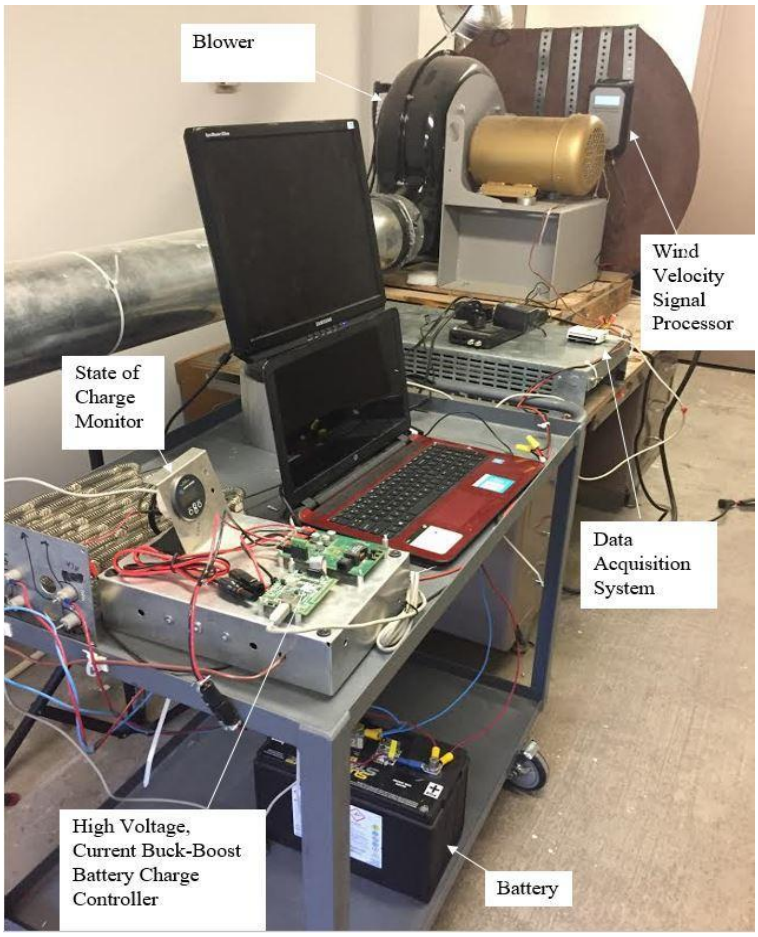

Figure 12-Wind turbine test rig (second view)

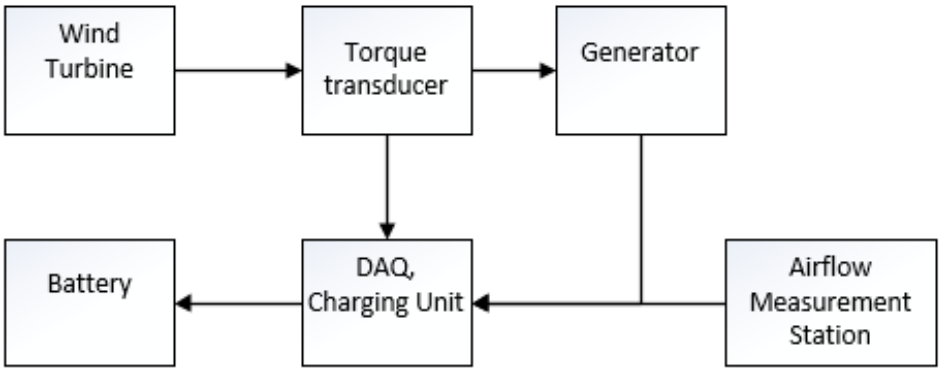

Figure 13-Schematic for charging system

3.1 Wind tunnel

The wind tunnel was designed so that it could produce a 50 mph wind speed over an area larger than the wind turbine blade diameter of 7 inches. After looking at several blowers and fans, an 8 in diameter was found to be the most appropriate to achieve the desire wind speed. A device called an Airflow Measurement Station, from Paragon Controls, was used to measure the average wind velocity going the wind tunnel. AMCA standard 210 specified that a length of ducting equal to 10 times the outlet diameter (80 inches) before the device and 32" after the device was required to have an accurate wind speed measurement, as shown in Figure 14.

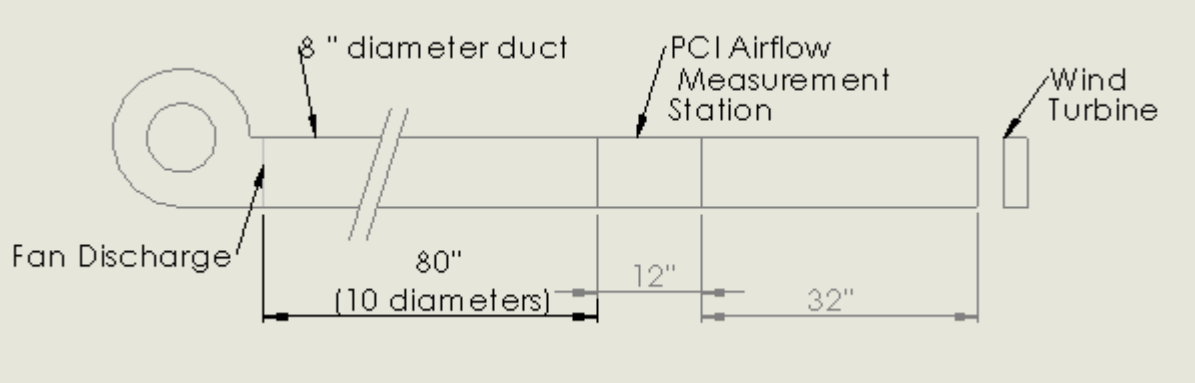

Figure 14-Sketch for AMCA standard 210

The first step in the design of the wind tunnel was to find a fan capable of producing the assumed 50 mph wind at a radius of about 8 inches which was slightly larger than the assumed wind turbine diameter of 6 in. A heavy duty blower with capability of delivering 2,400 CFM in an 8 in diameter was chosen, shown in Figure 15. Looking at the performance curve shown in Figure 16, this blower would deliver a max wind speed of V=Q/A=2,400 CFM/(pi*(8in)^2/4)=78 mph at the outlet (no resistance).

Figure 15-Heavy duty blower for wind tunnel, 8 in diameter outlet

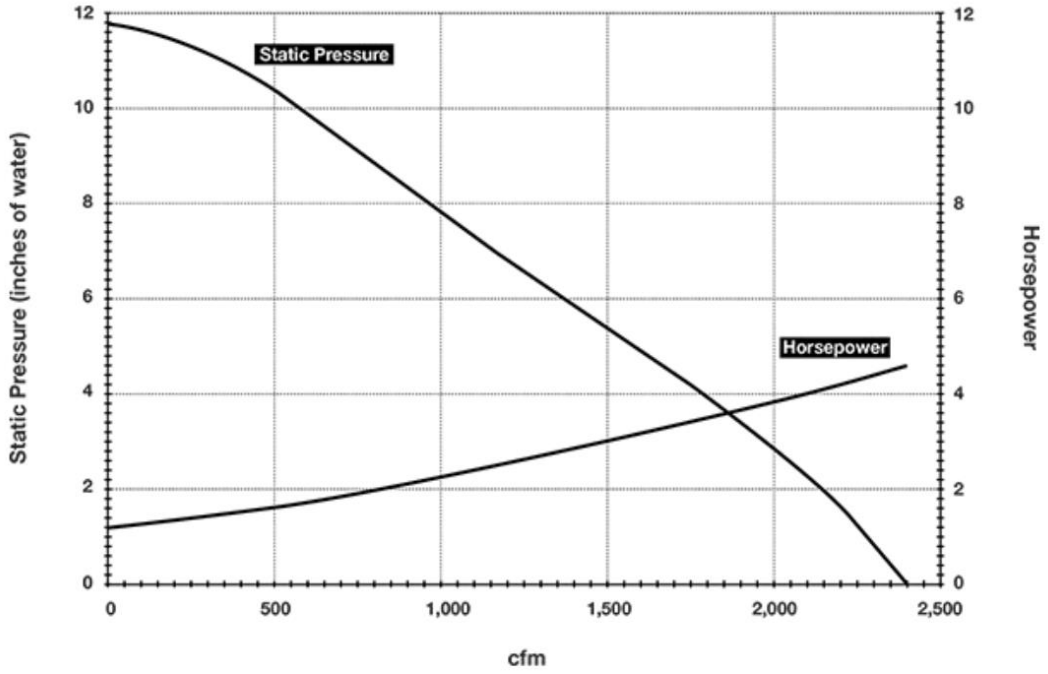

Figure 16-Blower performance curve at 3450 RPM

The next step in designing this blower was to be able to get a laminar flow and to be able to measure the average wind speed. A device that could make traverse measurements of a duct was chosen from Paragon Controls; an airflow measurement station. A traverse being an average

measurement of total and static pressures on the circular area, Figure 17 shows points of measurement on a circular area.

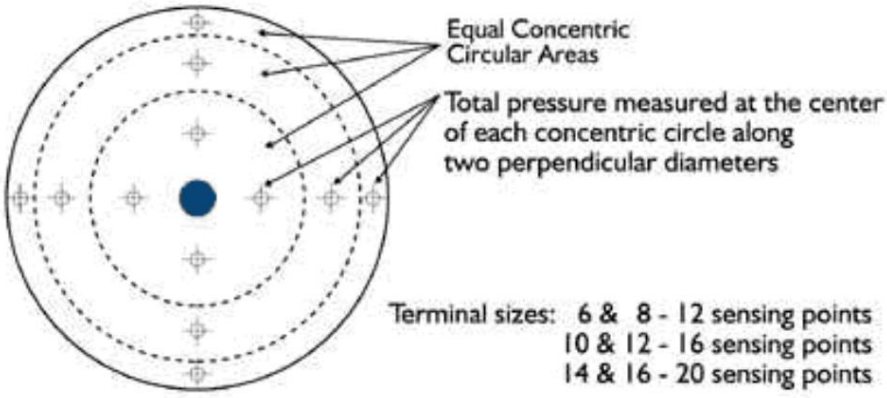

Figure 17-Traverse of a duct

Figure 18 and Figure 19 shows a schematic and drawing of the airflow measurements stations used for the wind tunnel. A duct with length equal to 10 times the blower outlet diameter was added between the blower outlet and the airflow measurement station in order to have an accurate airflow measurement, following AMCA standard 210 for airflow measurement; similarly a duct with length equal to 2.5 times the outlet was added to the outlet of the station, as shown in Figure 14.

Circular Stations

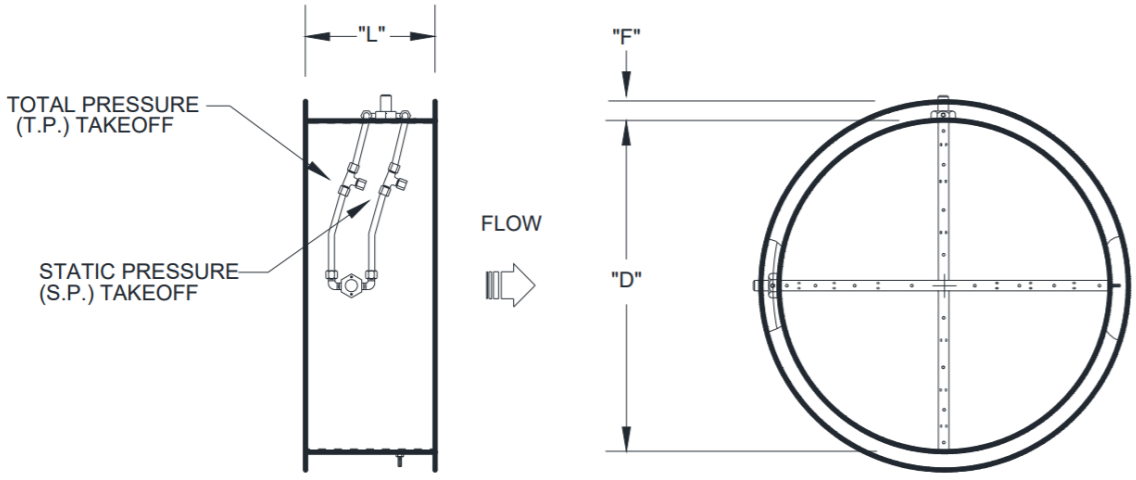

Figure 18-Schematic for circular airflow measurement station

Figure 19-Airflow measurement stations from Paragon Controls

A MicroTrans Signal Processors, shown in Figure 20, was used to read the voltage output of the airflow measurement station. The device provided a 0-5V output which corresponded to 0-50 mph wind velocity; this output was then connected to the DAQ system.

Figure 20-Wind speed signal processor "MicroTransEQ Signal Processor"

The last component for the wind tunnel was a variable frequency drive, shown in Figure 21, which was used to be able to vary the wind velocity coming out from the heavy duty blower.

Figure 21-Variable frequency drive

3.2 Wind turbine fixtures (bumper bearings, torque sensor, generator)

As previously stated, it was of interest to be able to measure the torque generated by the wind turbine blade at a given wind speed and angular velocity. A maximum torque of around 0.1 N-m was estimated for a 7 in wind turbine blade operating under a 50 mph wind and an angular velocity ranging from 0-10,000 RPM. Therefore, a rotary torque transducer from Interface Force with rating of 0.2 N-m was chosen as shown in Figure 22. Later on, a reaction torque sensor (nonrotating or static) shown in Figure 23 with the same rating of 0.2 N-m was used.

Figure 22-Interface Force rotating torque transducer

Figure 23-Interface Force non-rotating torque transducer

A fixture that would be able to hold the torque transducer along with generator was designed in Solidworks as shown in Figure 24. For this setup, the wind turbine would be driving the generator and the torque transducer would be measuring the transmitted torque and angular velocity of the system. A bearing housing with bearings with an inner race with a diameter slightly larger than the wind turbine blade shaft diameter was added in order to protect from blade bursts that could damage the torque transducer.

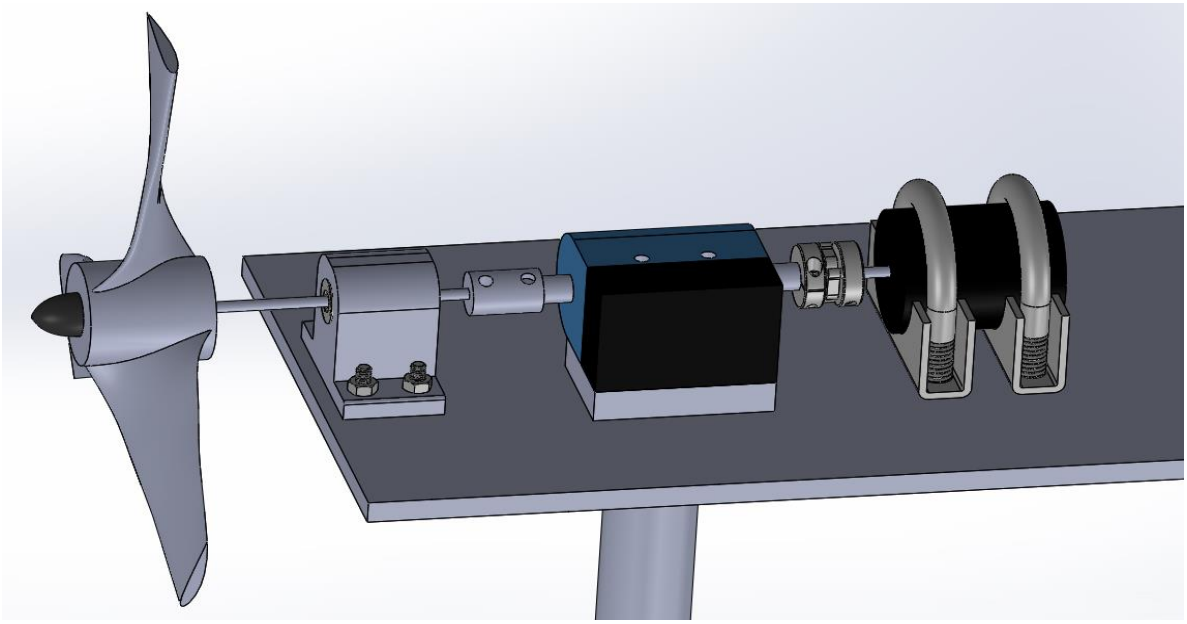

Figure 24-CAD model of wind turbine test fixture with rotating torque transducer

The components required for the fixture were machined and 3d printed. Figure 24 shows the assembled setup. The setup was placed in front of the wind tunnel and later on was used to test the wind turbine system.

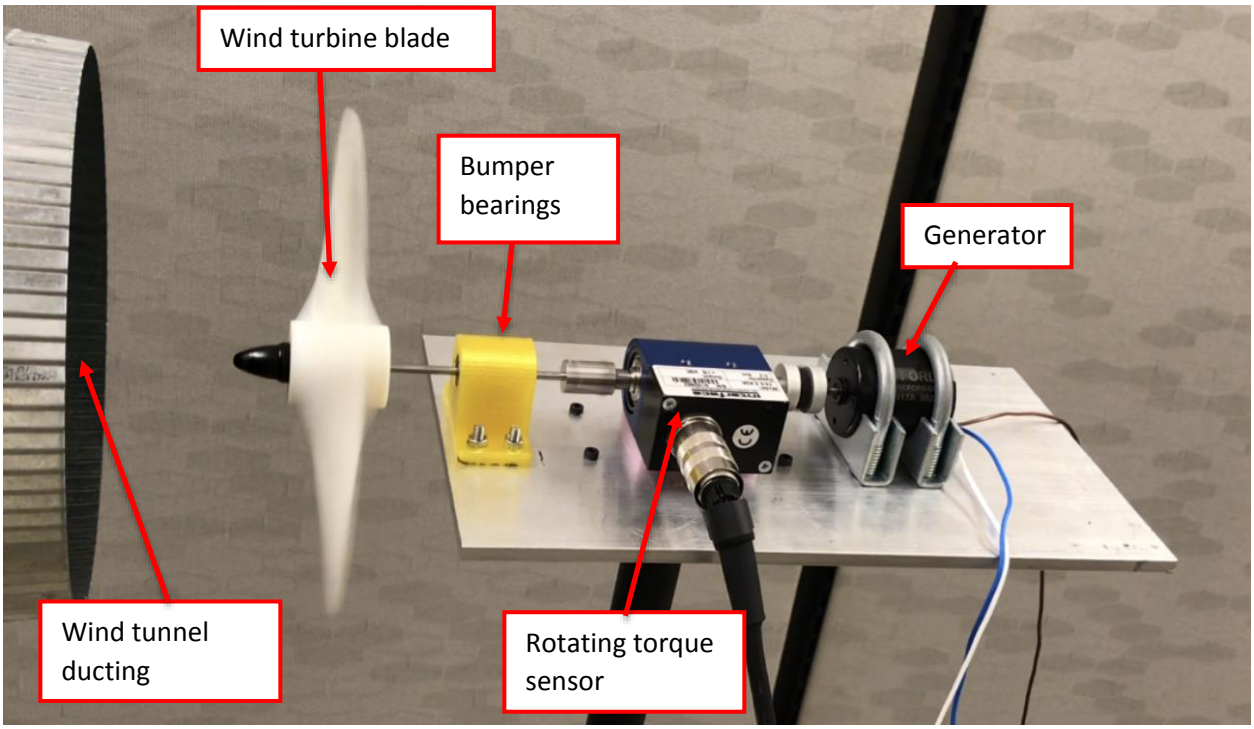

Figure 25-Assembled wind turbine test fixture with rotating torque transducer

A second fixture that would use a reaction (or static) torque sensor was designed using Solidworks as shown in Figure 26 and Figure 27. The difference between a reaction torque sensor and the torque transducer is that the first doesn't have rotating parts, while the latter does. Components were 3d printed and mounted on an aluminum plate; final assembly is shown in Figure *28*.

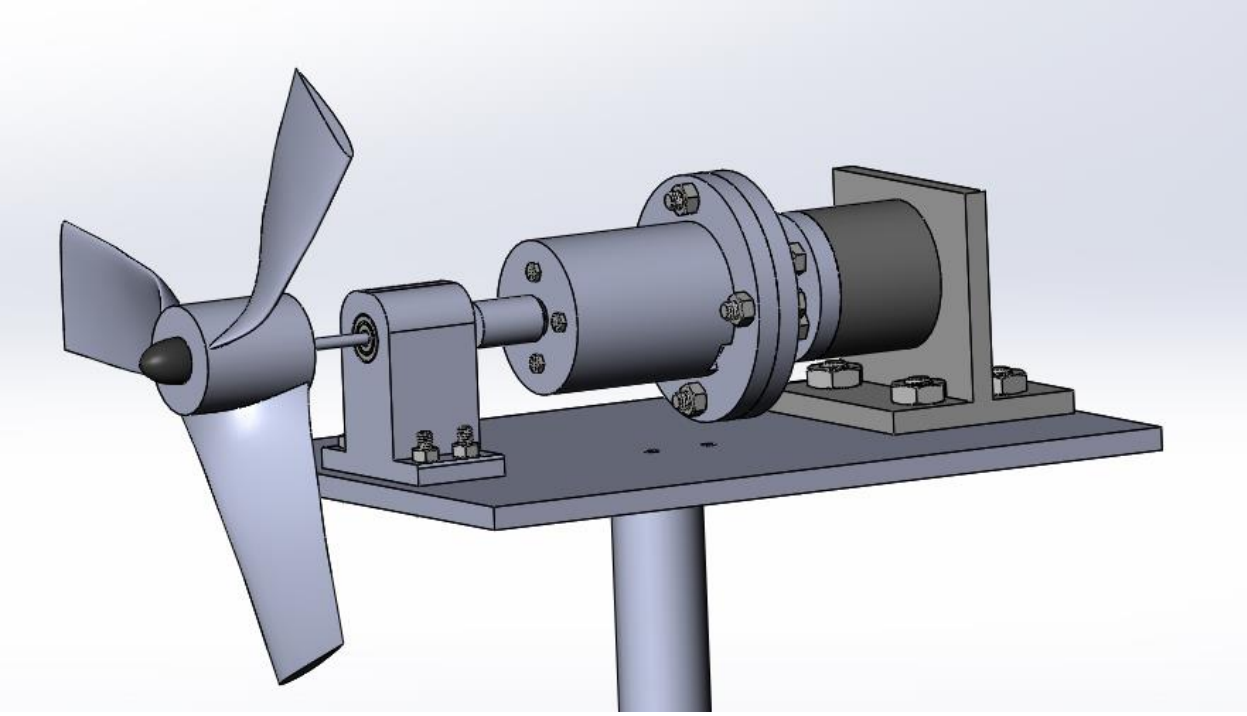

Figure 26-CAD model of wind turbine test fixture with reaction (non-rotating) torque transducer

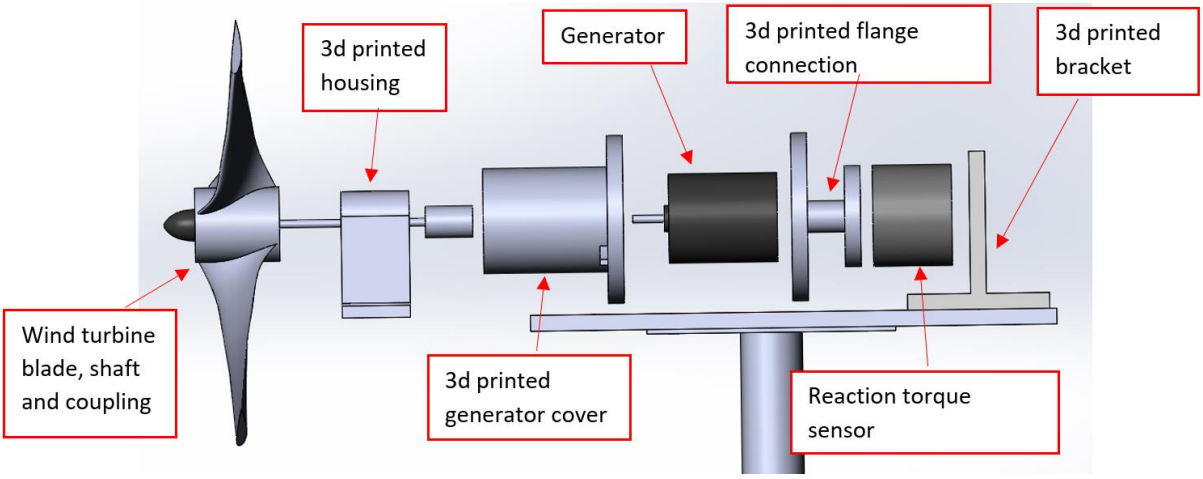

Figure 27-Exploded view of wind turbine test fixture with reaction (non-rotating) torque transducer

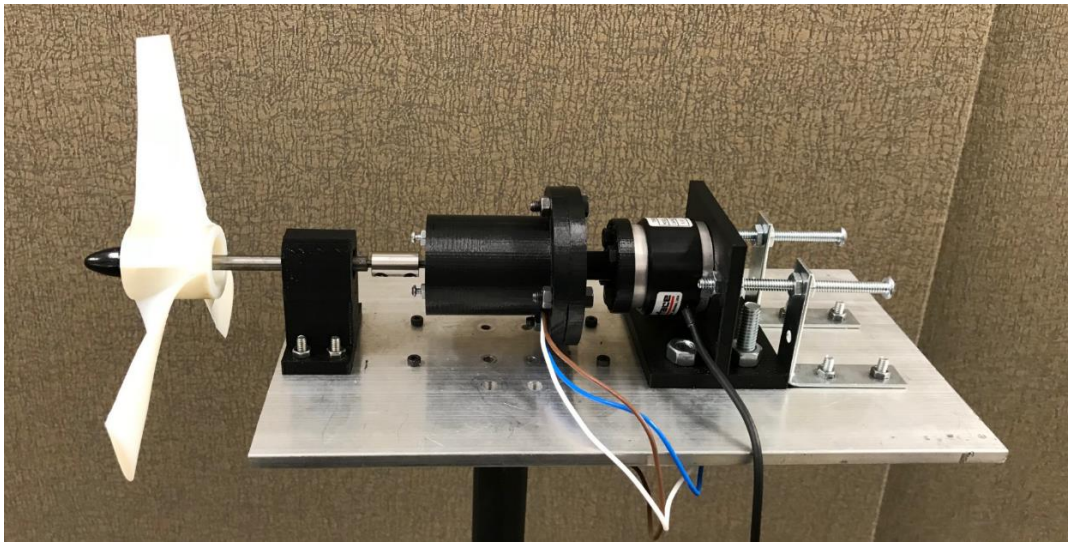

Figure 28-Assembled wind turbine test fixture with reaction (non-rotating) torque transducer

3.3 Charging system and data acquisition

The charging system is composed of the wind turbine 3 phase motor-generator, at which the wind turbine blade is mounted; a power converter to switch from AC to DC power; a charging unit; a 175 A-h 12 V lead acid battery; and a battery State of charge (SOC) monitor.

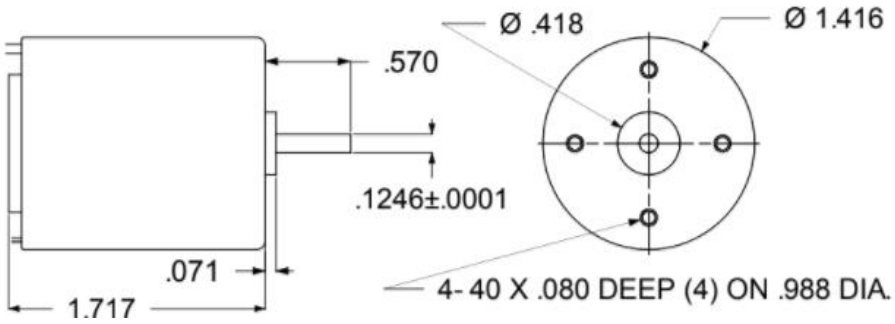

Figure 29-Koford motor model 36S417A dimensions

The motor/generator was chosen so it could be operated up to 10,000 RPM, had a minimum of 3 phases and that it had a size comparable to the 7 in chosen blade diameter. A permanent magnet

synchronous motor-generator with model # 36S417 A was chosen from Koford Engineering, LLC as with dimensions shown in Figure 29 and motor data and specifications shown in Table 1.

Table 1-Specifications for Koford motor/generator model 36S417A

Winding		**417**
Nominal supply voltage	volts	24
No load speed	rpm	10,000
Maximum efficiency	%	87
Continuous torque heat sink/no h.s.	oz-in	20/9.8
Motor constant Km	oz-in/vw	3.14
Winding resistance	ohm±15%	1.04
Peak output	watts	121
No load current	amp±50%	0.1
Damping factor	oz-in/krpm	0.025
Static friction	oz-in	0.076
Velocity constant	rpm/volt±12%	417
Torque constant Kt	oz-in/amp	3.2
Stall current	amps	23
Stall torque	oz-in	66.1
Winding inductance	mH	0.432
Mechanical time constant	ms	6
Rotor inerta	10-4oz-in-sec2	3.1
Thermal res. winding to case	°C/W	1.9
Thermal res case to ambient	°C/W	5.7
Bearing rating dynamic	Lb	71
Bearing rating axial (static)	Lb	29
Rated winding temperature	°C	150

A power inverter was designed and built to convert motor-generator AC power into DC power. Next, a charging unit that would condition the DC voltage and current coming from the power inverter was chosen from Linear Technology. The conditioning of DC voltage and current is helpful in that it maximizes the life of the lead acid battery since the charging unit changes the charge type depending on the state of charge of the battery. Figure 30 shows Linear technology components of the charging unit for the wind turbine system.

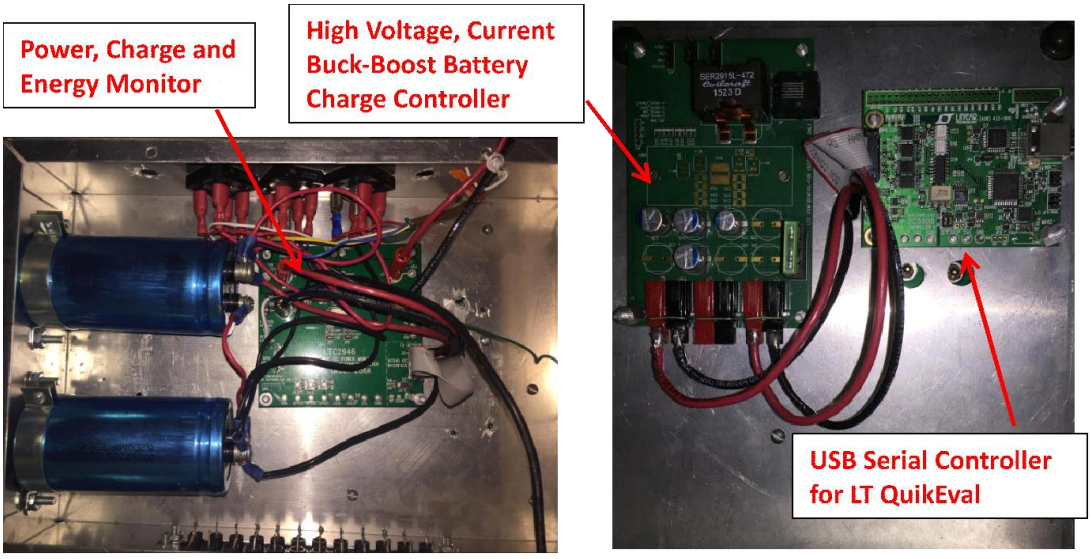

Figure 30-Charging unit components

Figure 31-Battery with 175 A-h capacity

A 175 A-h battery lead acid battery, shown in Figure 31, was chosen for this application. Commercial battery monitor was chosen from Victron, model BMV-702 shown in Figure 32 and was used to check the state of charge (or percent charge) of the battery. The battery monitor calculates the ampere hours consumed and the state of charge of the 175 A-h lead acid

battery. The ampere hours consumed are calculated by integrating the current flowing in and out of the battery.

Figure 32-Victron BMV-702 battery state of charge (SOC) monitor

Figure 33 shows a schematic of the charging system with discussed components

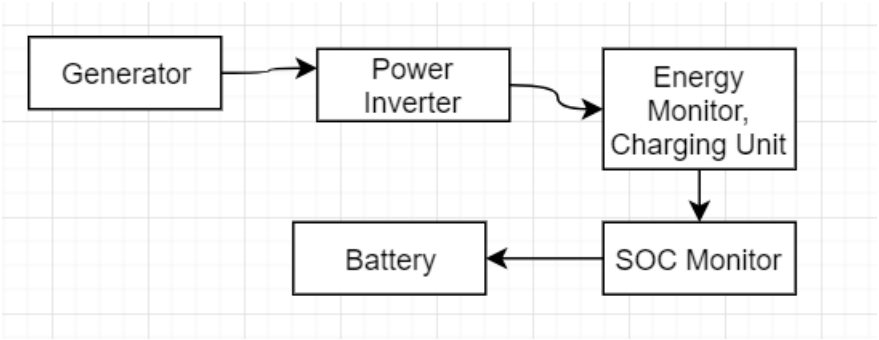

Figure 33-Schematic of charging system

A speed limiter circuit was also added to the charging system to prevent the wind turbine from rotating at high angular velocities when the battery SOC changes; this is helpful in preventing high rotational speed induced loads on the 3d printed blades and high vibrations that could damage the equipment. Figure 34 shows the speed limiter circuit.

Figure 34-Speed limiter circuit

The USB 6009 DAQ card is used for the data acquisition of the test rig, shown in Figure 35. Voltage output from the airflow measurement station, generator and torque sensors are connected to the card. LabVIEW software is used to analyze and store acquired data.

Figure 35-Data acquisition card USB 6009

4. PRELIMINARY TESTING

In this section, the testing of the charging system is presented and results for battery charging presented. From the design approach in section 1.2, it was mentioned that the electrical system torque and power curves would be matched to blade torque and power curves. The intersection between experimental electrical and theoretical blade curves would be than used as a design point for which an optimal blade would be designed, manufactured and tested. In these section, the setup and testing done to obtain electrical torque and power curves are discussed.

4.1 Charging of battery using wind turbine and solar panel

The charging system was tested to check rate of charge of battery was done using a solar panel and non-optimized 6 wind turbine blade. First, the charging of the battery is done using a solar panel. Afterwards, the battery is charged using a wind turbine. It is important that 2 methods were used to check the state of charge (or percent charge) of the battery.

For the charging using the solar panel, the battery voltage of the battery was checked to determine the state of charge of the battery. For the charging using the wind turbine, the Victron BMV-702 was used to check the state of charge monitor.

The state of charge results obtained using the battery voltage (charging using solar panel) might be inaccurate since it might take hours for this voltage to normalize, whereas the voltage was measured after just 2 minutes.

4.1.1 Charging of battery using solar panel

The solar panels in Figure 36 were connected to the charging system following schematic shown in Figure 37. For this test, the solar panels were placed outdoors. The battery was charged for ten minutes and then disconnected from the charging unit. The battery was left to rest for about 2 minutes and the battery voltage was measured. This was repeated 6 times for a total charging time of 1 hour

Figure 36-Solar panels

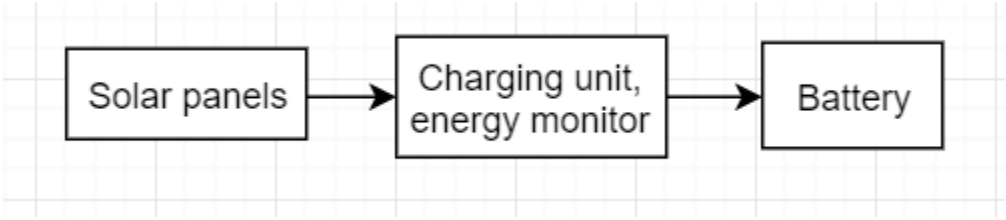

Figure 37-Setup for charging of battery using solar panels

Figure 38 shows the charging of the battery results for a test that lasted for 1 hours. These results might not be accurate since the battery was left to rest for 2 minutes after being charged, to check the state of charge voltage; a battery should be left resting for a couple of hours in order for the state of charge voltage to normalize and be accurate.

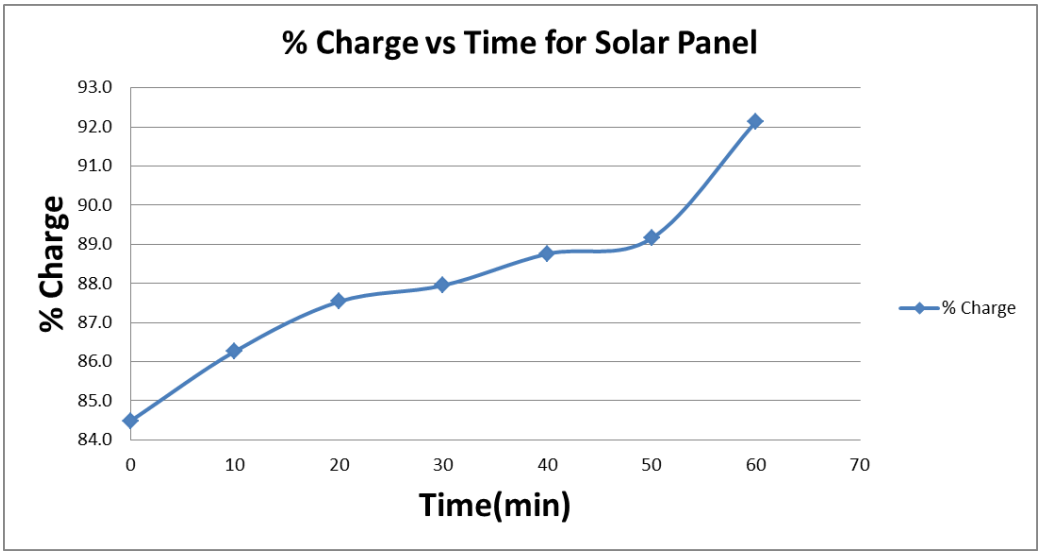

Figure 38-Charging of battery using solar panel results

4.1.2 Charging of battery using wind turbine

Testing of the charging system was done using a non-optimal wind turbine blade to check the charging rate of the battery. The charging rate was monitored by the BMV-702 Victron battery monitor which track Amp-hours used by integrating current going in and out of the battery. The wind tunnel was run at 50 mph and a 6 inch wind turbine blade was used for this experiment. Figure 39 shows the setup used for this experiment.

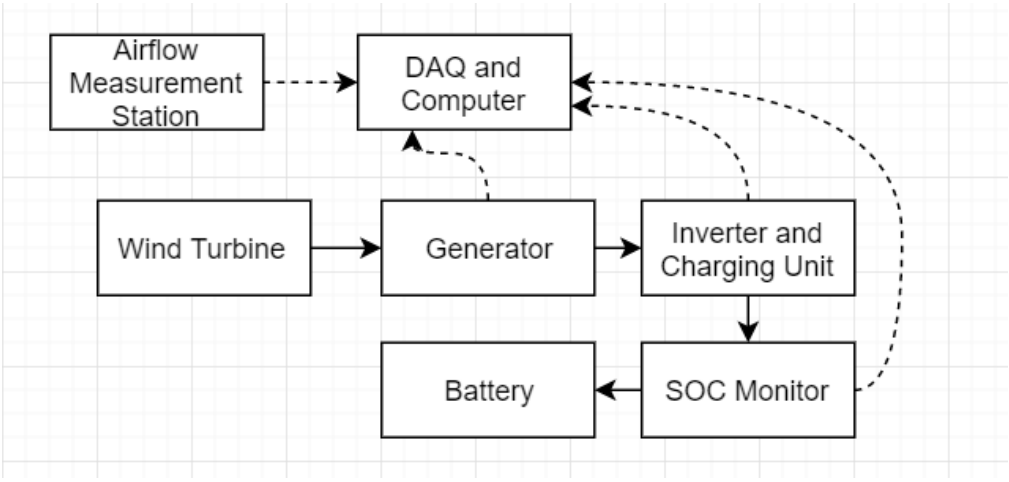

Figure 39-Setup for charging of battery using wind turbine

Figure 40 shows the results of the charging of the battery. The test duration was 170 minutes and the battery was charged from 95% to 97.6%, which corresponds to around 4.55 A-h charged.

The line isn't smooth due to the monitor only measuring in 0.1% increments; it took about 6-7 for each state of charge to change by 0.1%.

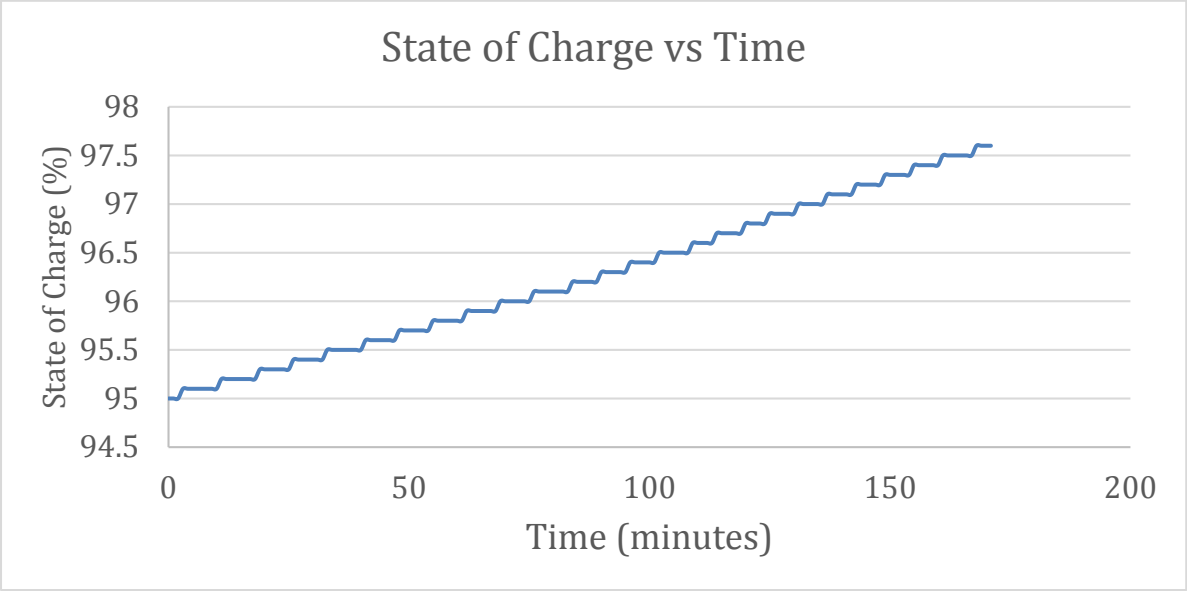

Figure 40-Charging of battery with wind turbine results

4.2 Torque and power curves generation for electrical system

Now that the battery charging system was tested, a setup consisting of a motor driving the wind turbine generator with a torque transducer in between was built as shown Figure 41. The applied torque at a given angular different velocities was measured while the generator was connected to the charging unit and battery as shown in schematic in Figure 42.

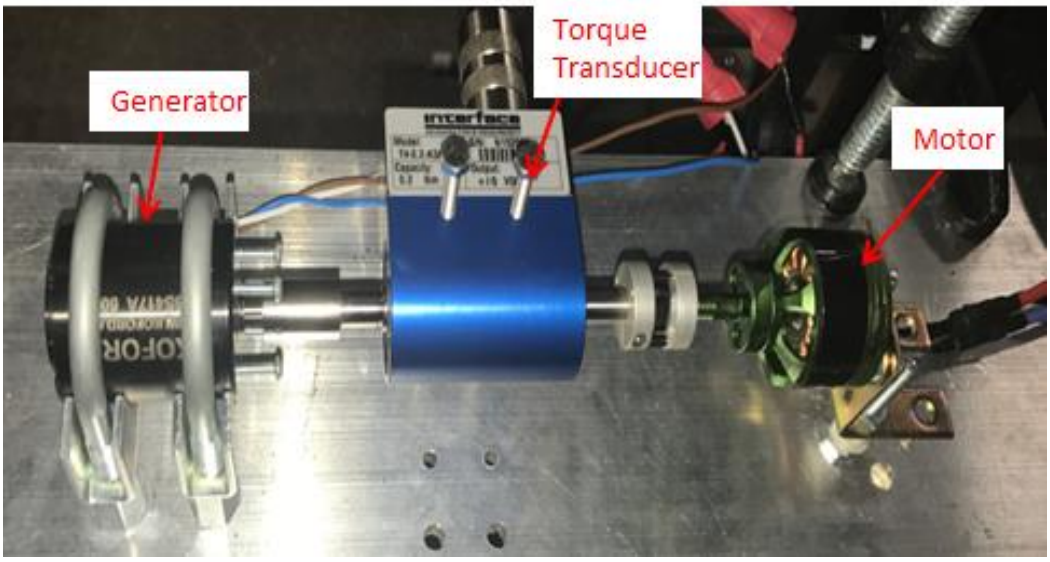

Figure 41-Fixture used to produce electrical system characteristic curves, motor drives system

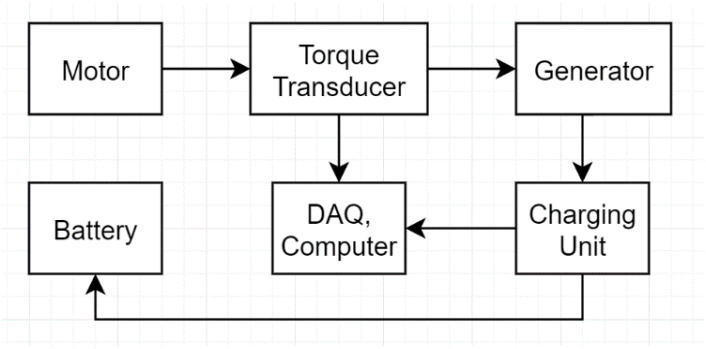

Figure 42-Schematic of system used to create electrical system torque and power characteristic curves

The Victron battery monitor was used to check the SOC of the battery when charged and discharged. The experiment was done at 80, 85,90,95,99 and 100% SOC'; battery was discharged using a resistor bank. It is recommended not go below 80% SOC to maximize the life of the battery. Figure 43 shows the results for the experiments. The curves for the 95-100% SOC have a shorter RPM range due to the system rotating much faster after certain speeds (5500 RPM and 0-6000 RPM); the reason being the charging unit changes the mode of charge. The system was shut down after this sudden increase in velocity to protect the torque transducer which has a limit of 10,000 RPM.

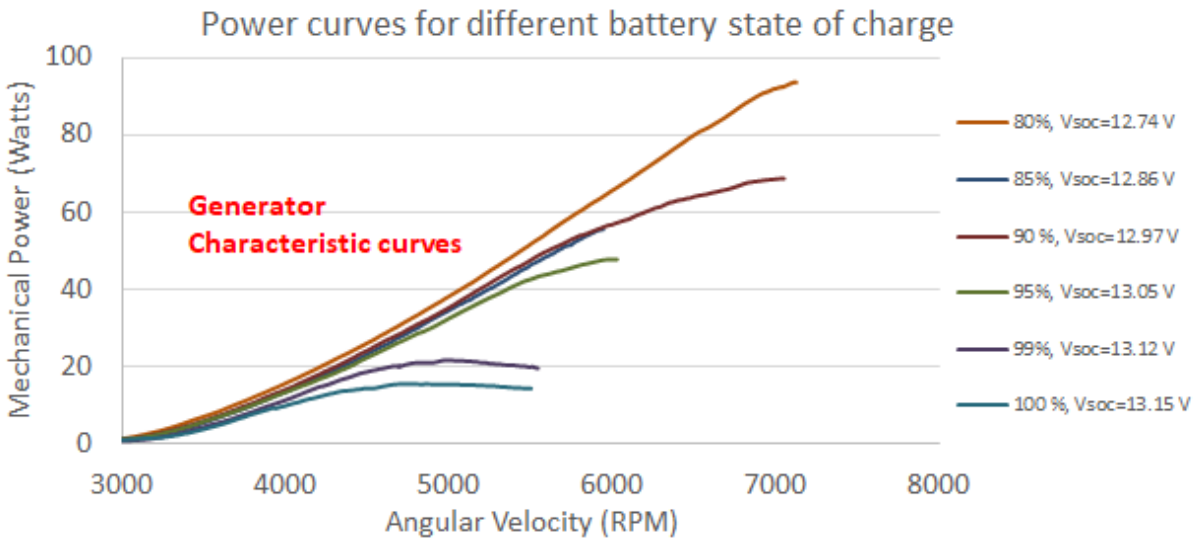

Figure 43-Electrical system characteristic curves

Figure 43 shows that as the SOC decreases, the maximum mechanical power increases. Therefore, the aim of the wind turbine design would be to be able to operate at all these ranges. The next step is to obtain theoretical blade curves and correlate with the electrical charging system curves.

5. MODELING AND SIMULATION

The purpose of this section is to discuss the computational modeling and/or simulation performed to obtain the optimal location of a wind turbine on top of a car, theoretical blade characteristic curves, the choice, modeling and manufacture of optimal blade design for desired application, and stress analysis of chosen optimal blade design. First, computational fluid dynamics analyses are performed to check the wind velocity of a train car; Mecaflux Heliciel software is introduced and used to obtain blade characteristic curves, an optimal blade design is chosen, defined and drawn in Solidworks; and the chosen optimal blade design is analyzed using stress FEA using ANSYS Structural software.

5.1 Computational fluid dynamics (CFD) analysis

5.1.1 CFD simulation of train cars

The purpose of this computational fluid dynamics (CFD) analysis was to model a 6 train car model in ANSYS CFX to determine velocity profiles on top of the trains and determine the wind speed perceived by a wind turbine on top of a train car. After the initial analysis, it was determined that the wind velocity close to the top surface of the train cars was below 50 mph. A second analysis was performed in which a bump or a shroud was added on top of the 3rd car to determine the increase of wind speed at the top surface of the train cars. The first analysis CFX results showed that at the 4th or 5th car, the wind speed perceived by the wind turbine would be 39 mph and 40 mph, respectively, at 1 ft above the train (results shown in Figure 50. The second analysis shows that there's an area of relative velocity higher or equal to 50 mph close to 1-1.5 ft above the top surface of the train, next to the bump (results shown in Figure 53).

The train cars solid model was created in Solidworks. The dimension of each train car was assumed to be 50 ft long, 15 ft high and 10 feet wide; the distance between each car was assumed to be 4 ft. Figure 44 and Figure 45 show the drawings for the no bump and bump case respectively.

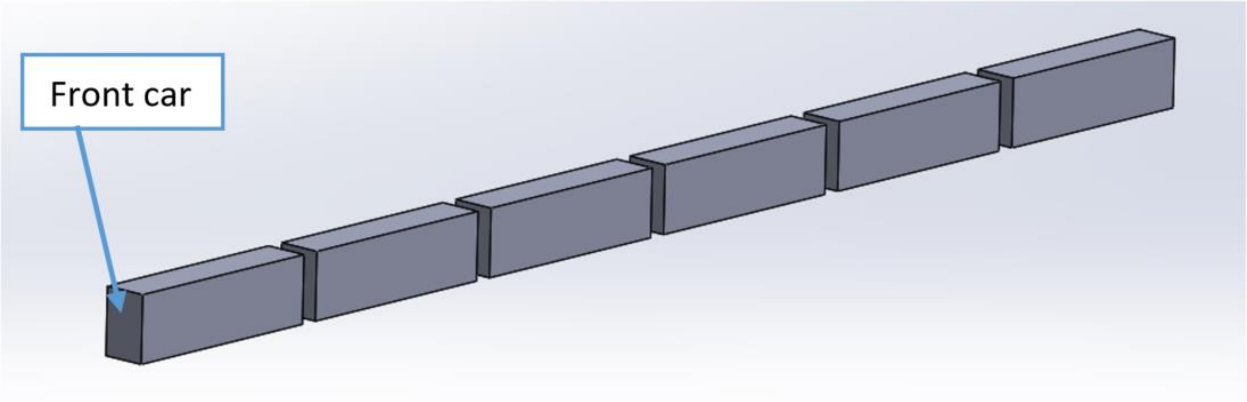

Figure 44-Solidworks drawing of train cars, without bump

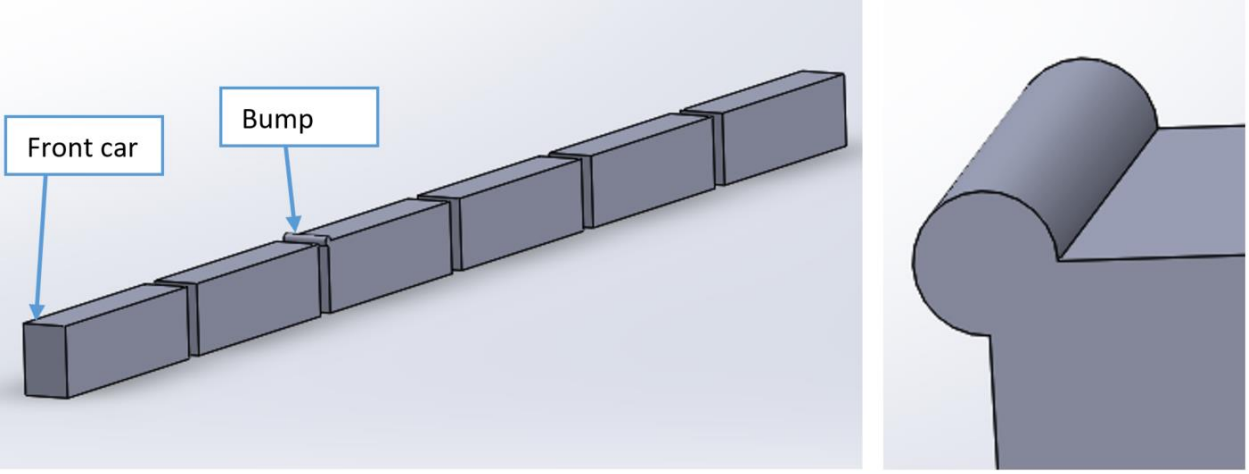

Figure 45-Left: Solidworks drawing of train cars with bump, right: zoomed in bump

The Solidworks CAD drawing was then imported into computational fluid dynamics (CFD) software CFX. The train cars were placed in an enclosure and symmetry was assumed to reduce computation time. The model was meshed using the CFX built in function, which resulted in ~450,000 elements. The fluid was assumed to be air at 25 degrees Celsius and reference pressure of 1 atm. An inlet velocity of 50 mph was applied in the inlet while a relative pressure of 0 Pa was applied at the outlet; this would be a close approximation of the wind behavior if the train cars were moving and wind were static. Figure 46 shows the rest of the boundary conditions locations and wall definitions.

In this analysis, train cars are placed in a large enclosure volume. This enclosure volume would represent the fluid, or air, that surrounds the train cars. In this analysis, the train is stationary and the fluid is moving; when in real life is the opposite, the train car moves and the flow is stationary. However, the flow perceived by an object on top of the train can be determined by

applying the inlet velocity. If we wanted to analyze the flow perceived by an object on the side of a track, we would have to subtract the inlet velocity (in this case 50 mph) to the results of the analysis. Therefore, the flow going through a moving train car can be analyzed by applying an inlet velocity, shown in conditions Figure.

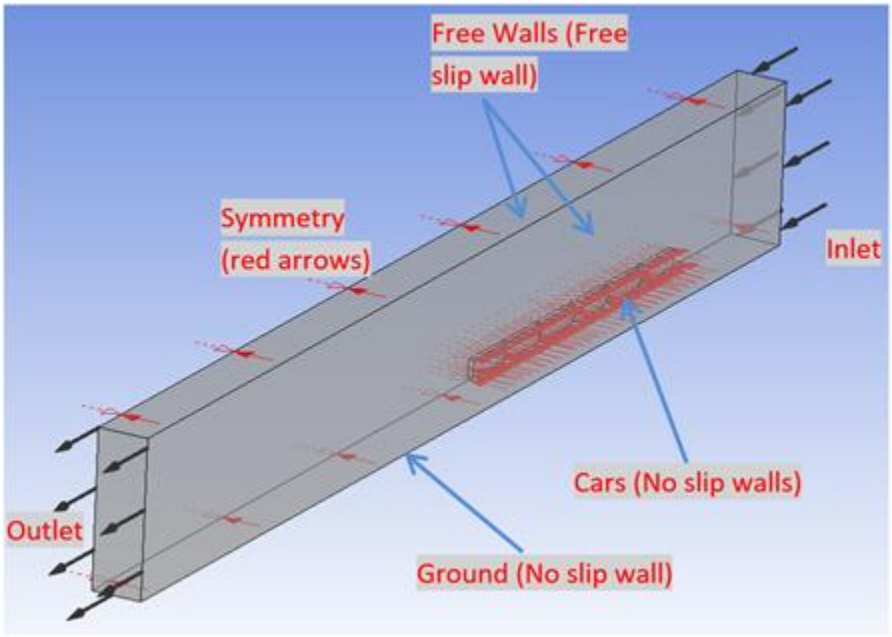

Figure 46-CFD of train cars boundary conditions

Results for model without bump

The model without bump simulation was run until the results converged. First, contour plots of relative velocity in the direction of the moving train; relative velocity being the wind velocity perceived by an object on top of the train. Figure 47 shows the relative velocity contour plot for the train cars along the symmetry plane, while Figure 48 shows the same contour plot but zoomed in to the 4^{th} and 5^{th} car.

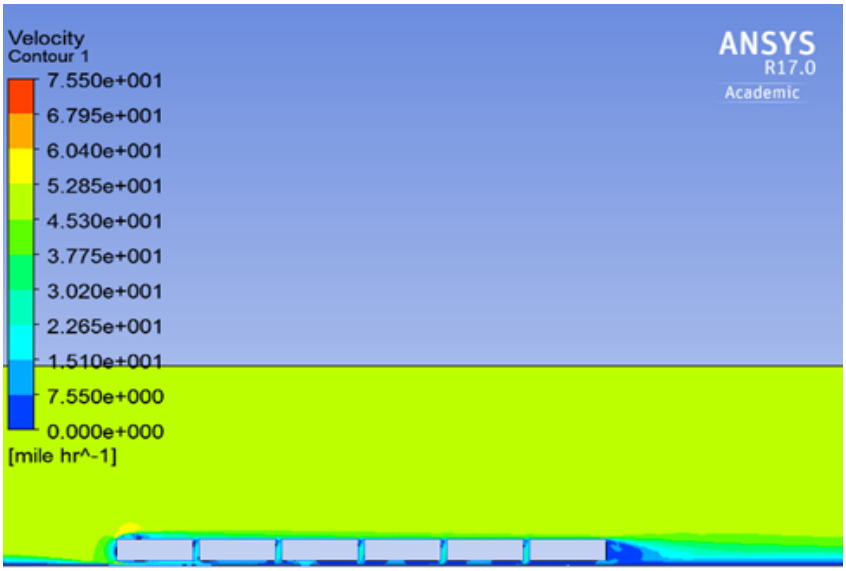

Figure 47-Relative velocity contour plot for 6 train car model (front train is on left)

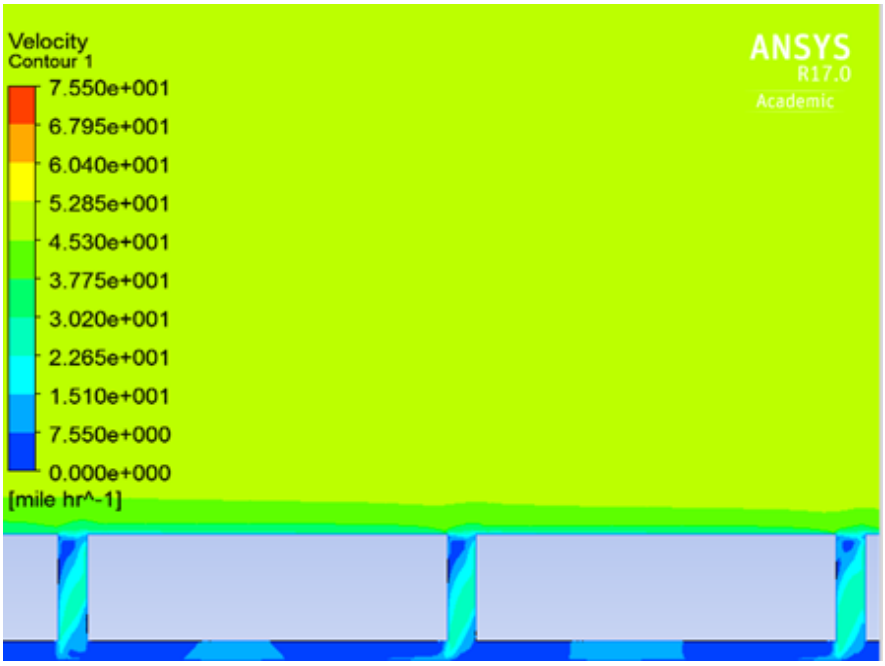

Figure 48-Relative velocity contour plot zoomed in to 4th (left) and 5th car (right)

In order to compare the velocity profiles of the trains, 6 lines were created in trailing edges as shown in Figure 49. The velocity in the z direction vs the distance from the top of the train was plotted in Figure 50 for each of the previously defined locations or lines.

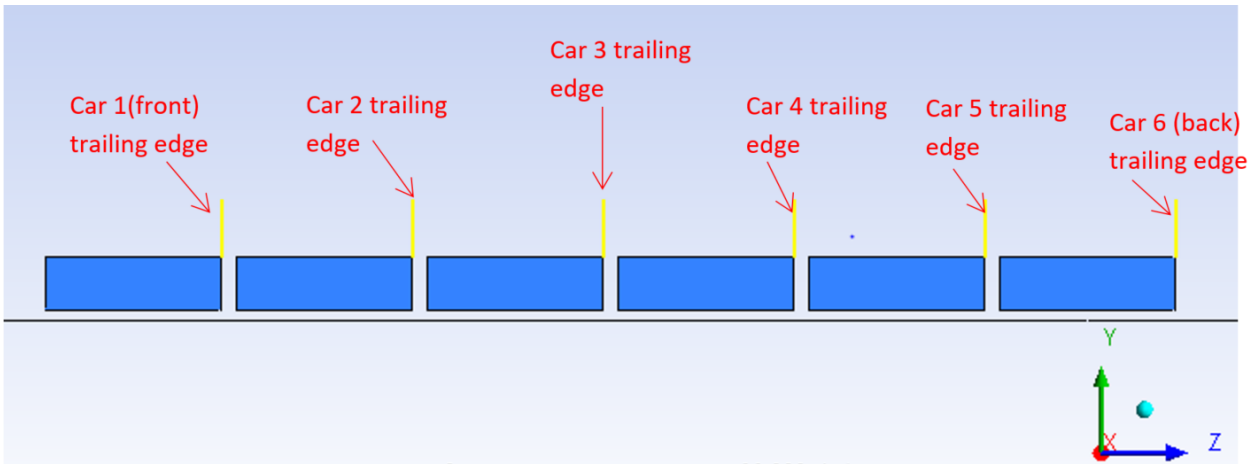

Figure 49-Lines were comparison of relative velocity profiles were made (shown in yellow)

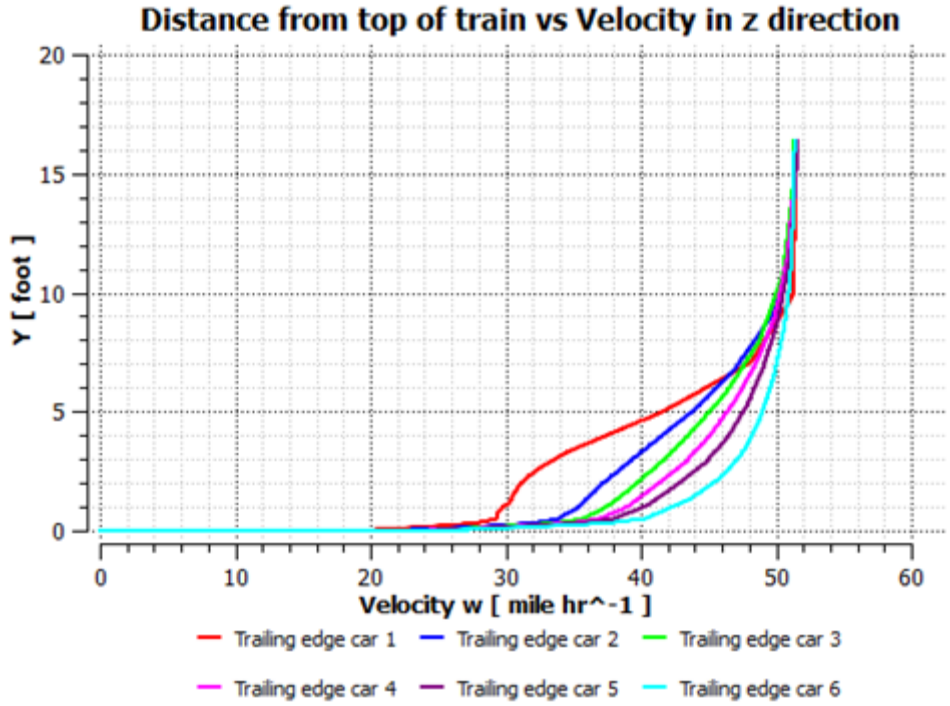

Figure 50-Comparison of relative velocity profiles for 6 train car model

Figure 50 (plotted lines at trailing edges) shows that a good location for a wind turbine would be at 1 ft above the top surface of the 4th and 5th car trailing edges since the wind velocity in the direction of the moving train is 40 mph (check clearance on top of train); where 'Y' is the distance from the top of the train car. In order to achieve the 50 mph wind velocity, the wind turbine would have to be placed close to 10 ft above the top surface of the train; however, there would be a problem if the train goes through tunnels.

Results for model with bump

Previous results showed that a wind velocity of 40 mph can be extracted close to 1 ft above the top surface of a train far behind the top train. A second model that includes a bump as previously discussed, shown in Figure 45, was simulated. Figure 51 shows a relative contour plot along the symmetry plane, zoomed in to the 3rd car where the bump.

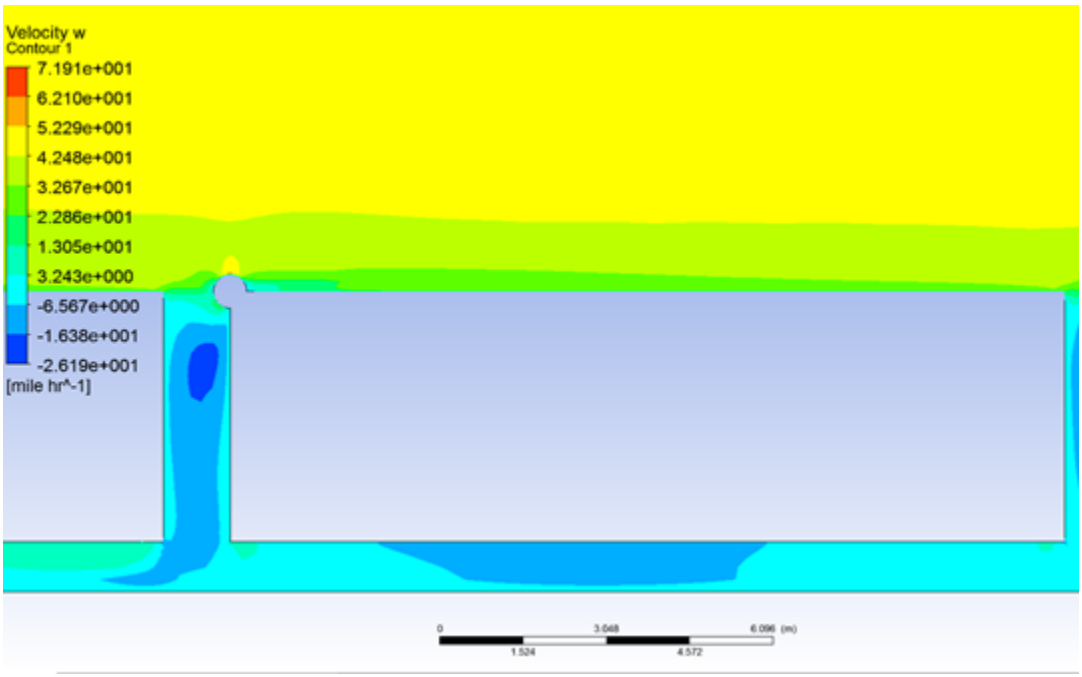

Figure 51-Relative velocity contour plot for model with bump on 3rd car

Figure 51 contour plot shows that there's an area with high velocity close to the top of the bump. Like the previous CFD analysis, 6 lines of comparison were created but in the front edge of the train cars as shown in Figure 52 (note that previous lines were in the back of the train). These lines will serve to compare the velocity close to the top surface of the train.

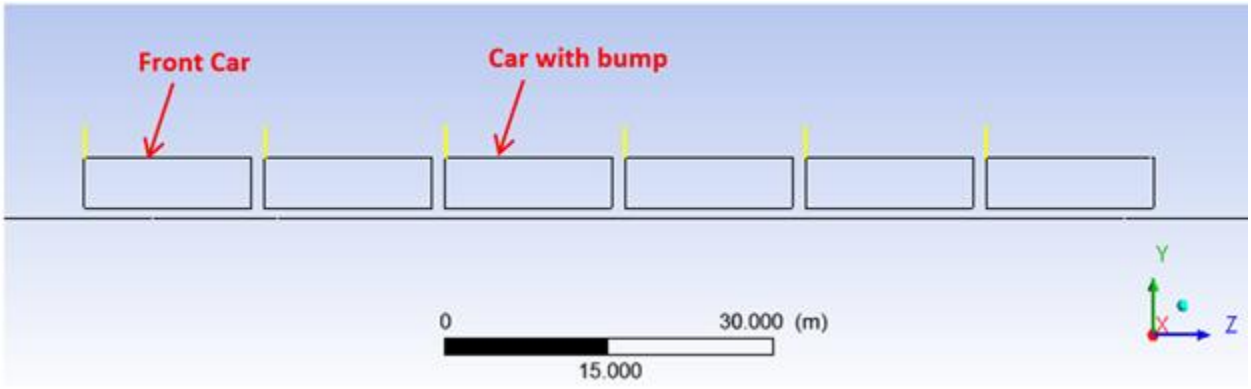

Figure 52-Location of lines (yellow) where wind speed (z-direction) was taken; for bump addition comparison

Figure 53 shows the relative velocity results in the direction of the moving train in the lines described above, where 'Y' is the distance from the top of the train car. The green line, for the car with the bump shows that there's an area of relative velocity higher or equal to 50 mph close to 1-1.5 ft above the top surface of the train, just above the bump. The wind turbine could be placed on top of the bump to harvest a more energy from the higher wind speed.

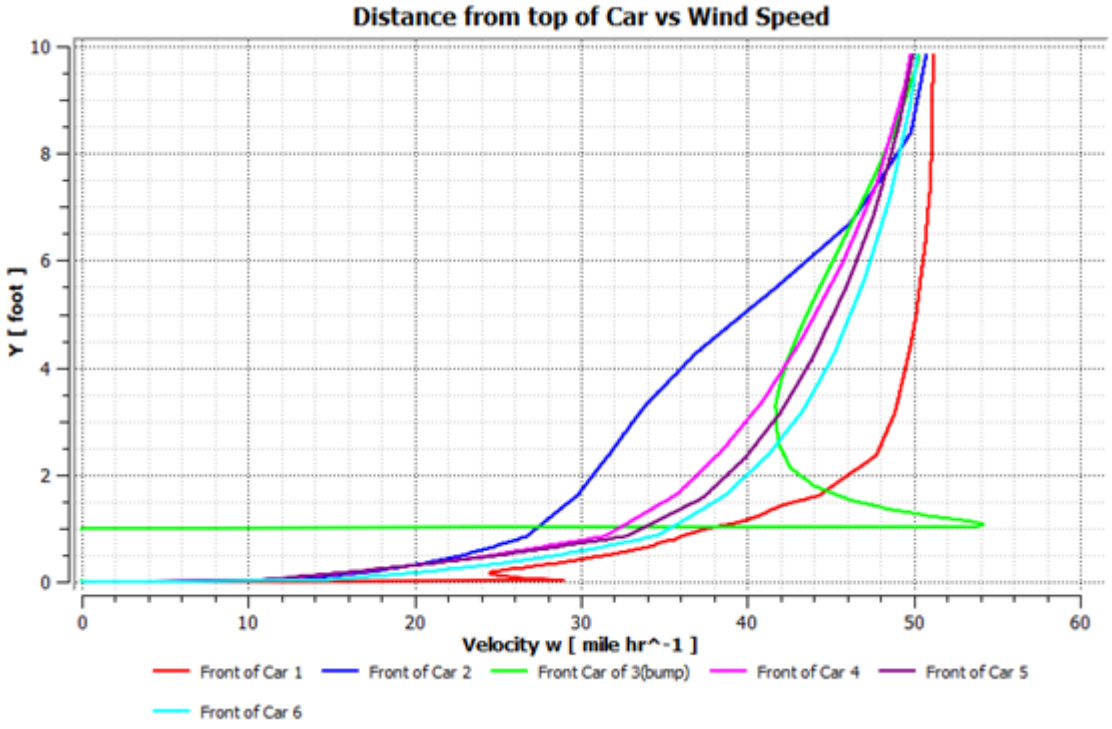

Figure 53-Distance from top of car vs relative wind velocity for bump model

5.1.2 CFD simulation of 6 inch wind turbine blade

The objective of this CFD analysis was to obtain torque (as well as power and efficiency) curves for a previously non-optimized 6 inch blade and compare to results from Blade Element Momentum (BEM) software Mecaflux Heliciel (discussed in section 5.2). Later on, the power loss effects of adding a cowling to the wind turbine, shown in Figure 60, is analyzed using CFD.

5.1.2.1 Convergence check and comparison to BEM results

A 6 inch diameter blade was drawn in Solidworks and imported to ANSYS Fluent. The blade was meshed into 3 different mesh sizes: coarse, medium and fine (0.5 million, 1 million, 1.5 million elements respectively). For the boundary conditions, the blade was placed in a disk slightly larger than the blades width and diameter as shown in Figure 54-Rotating volume of fluid (disk) for CFD analysis of 6 inch blade.

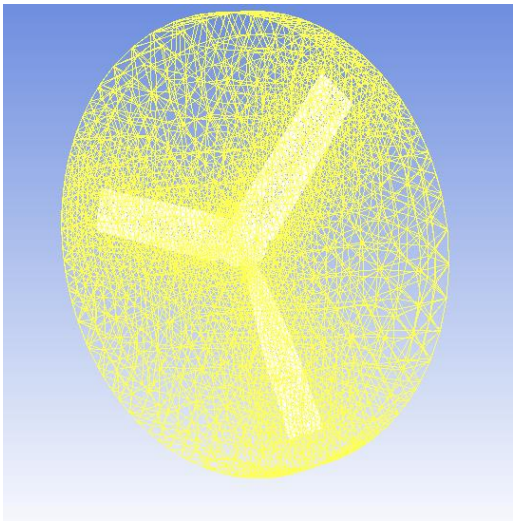

Figure 54-Rotating volume of fluid (disk) for CFD analysis of 6 inch blade

The blade is then placed in an enclosure as shown in Figure 55-Setup and boundary conditions for CFD analysis of wind turbine blade; the blue face represents the inlet where a velocity of 50 mph was applied; the white surface represents an enclosure to the blade, where the mesh remains static; the yellow surface represents the fluid around the 6 in wind turbine blade, this is the mesh section that rotates at the blades angular velocity; the red face represents the outlet where a 0 gauge pressure is applied. An operating pressure of 100,000 Pa is applied to the model. The material properties used are those of air with a density of 1.143 kg/m^3 and dynamic viscosity of

1.89x10^{-5} Pa/sec^2. For the convergence check/grid independence, an angular velocity of 10,000 RPM is applied to the yellow section initially.

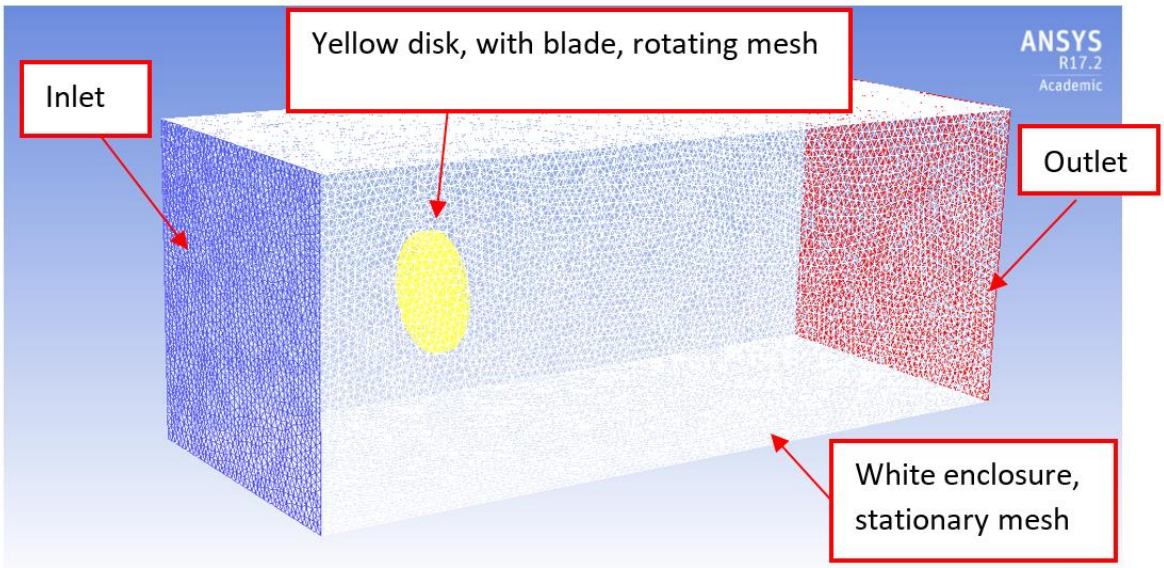

Figure 55-Setup and boundary conditions for CFD analysis of wind turbine blade

Table 2-CFD torque results for 6 inch blade at 3 mesh sizes and Figure 56-CFD torque results for 6 inch blade at 3 mesh sizes shows the torque results at different mesh sizes, for the 6 inch blade rotating at 10,000 RPM under a 50 mph wind. From these results, it was determined that 1 million elements is a good mesh size to run more analyses.

Table 2-CFD torque results for 6 inch blade at 3 mesh sizes, 50 mph wind and 10,000 RPM

Mesh	# elements/cells	torque (N-m)
coarse	~500,000	0.02761
medium	~1,000,000	0.04806
fine	~1,500,000	0.04784

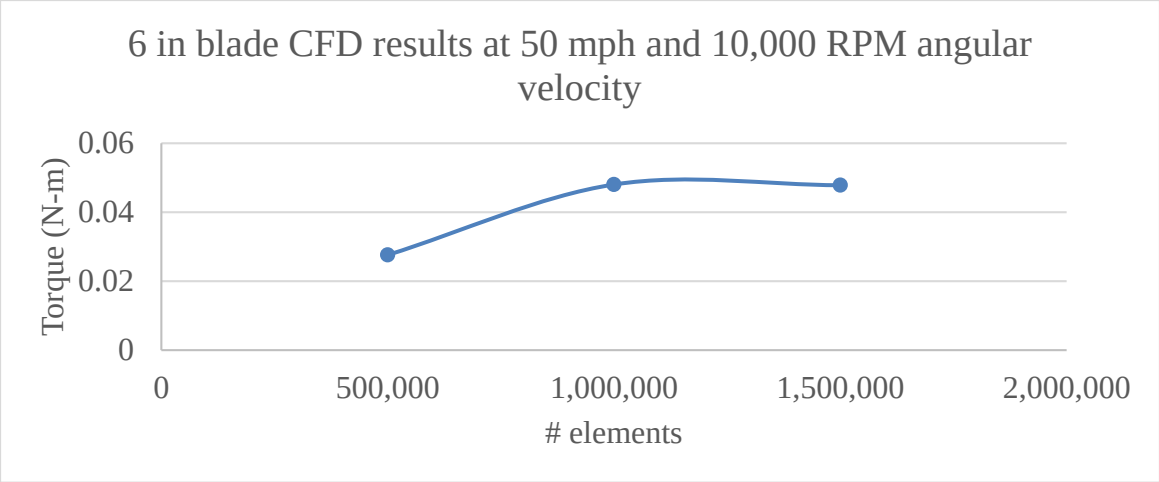

Figure 56-CFD torque results for 6 inch blade at 3 mesh sizes

Now, the same analysis is performed at 8,000-13,000 RPM range, and compared to results from Blade Element Momentum (BEM) software. Table 3 shows the CFD results for the analysis. Figure 57 and Figure 58 show the comparison between the Fluent CFD software and Heliciel BEM software torque and power results.

Table 3-CFD torque, power and efficiency results at 50 mph wind for 6 inch blade

Angular Velocity(RPM)	**CFD torque (N-m)**	**CFD Power (Watts)**	**Cp**
8000	0.0535	44.8	0.39
9000	0.0514	48.4	0.42
10000	0.0481	50.4	0.44
11000	0.0434	50.0	0.43
12000	0.0393	49.4	0.43
13000	0.0347	47.2	0.41

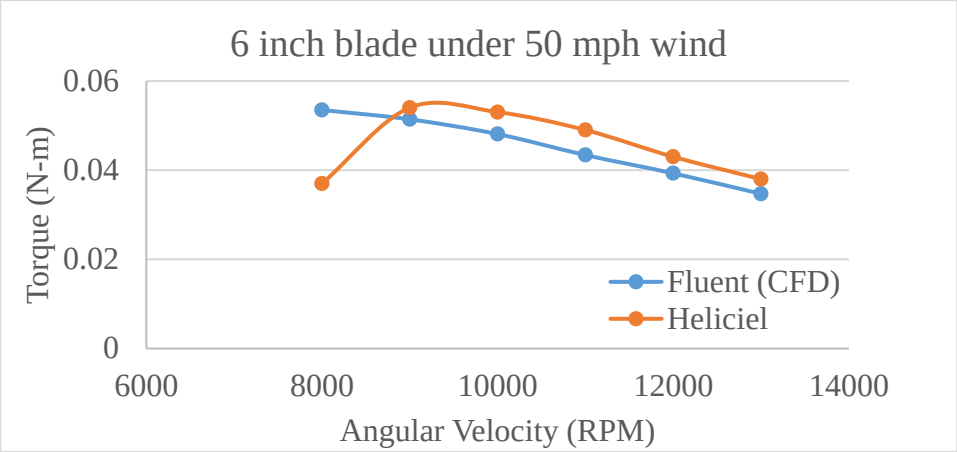

Figure 57-Torque curve comparison of Fluent (CFD) and Heliciel (BEM) results

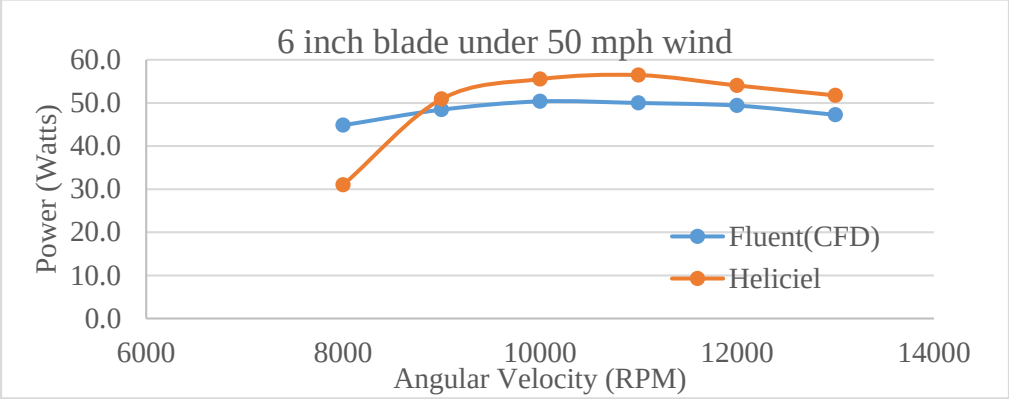

Figure 58-Power curve comparison of Fluent (CFD) and Heliciel (BEM) results

Table 4 shows a comparison of CFD power obtained from Fluent software to BEM power obtained from Heliciel software; percent difference is computed for each of the curve points. Torque and efficiency results would yield the same percent difference since results would be multiplied by a constant related to wind power and angular velocity. Percent difference average for power results is 13%; however, best thing would be to compare to torque power, and efficiency results obtained from an experiment performed on the blade. Figure 59 shows streamline results for a 6 inch blade when perceiving a 50 mph wind.

Table 4-Comparison of Fluent CFD and Heliciel BEM power results

Angular Velocity (RPM)	CFD power (watts)	Heliciel power (watts)	% diff
8000	44.8	31.0	31%
9000	48.4	50.9	5%
10000	50.4	55.5	10%
11000	50.0	56.4	13%
12000	49.4	54.0	9%
13000	47.2	51.7	10%

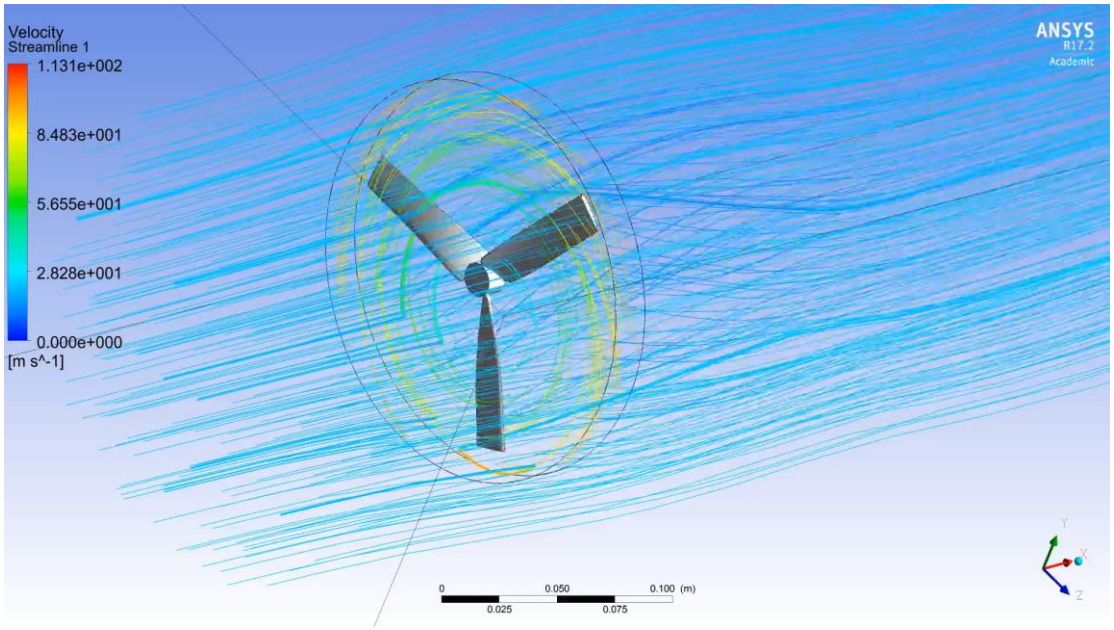

Figure 59-CFD streamlines results for 6 inch blade (video: https://youtu.be/zkEFaje69AA)

5.1.2.2 Power loss caused by cowling and generator

A cowling concept was developed as shown in Figure 60. The cowling would protect from objects such as birds or rocks that could get close to the wind turbine when attached to the top of a train car. Before the optimization of the 7 inch wind turbine blade, a CFD analysis was performed on a non-optimized 6 inch to determine the power loss effects caused by adding a cowling. The approach taken was to model and perform CFD analysis for several cases ranging from blade by itself, blade+generator, blade+generator+cowling, with different cowling designs(thinner, with slots); and then compare maximum power for each case and compare; plot torque and power curves.

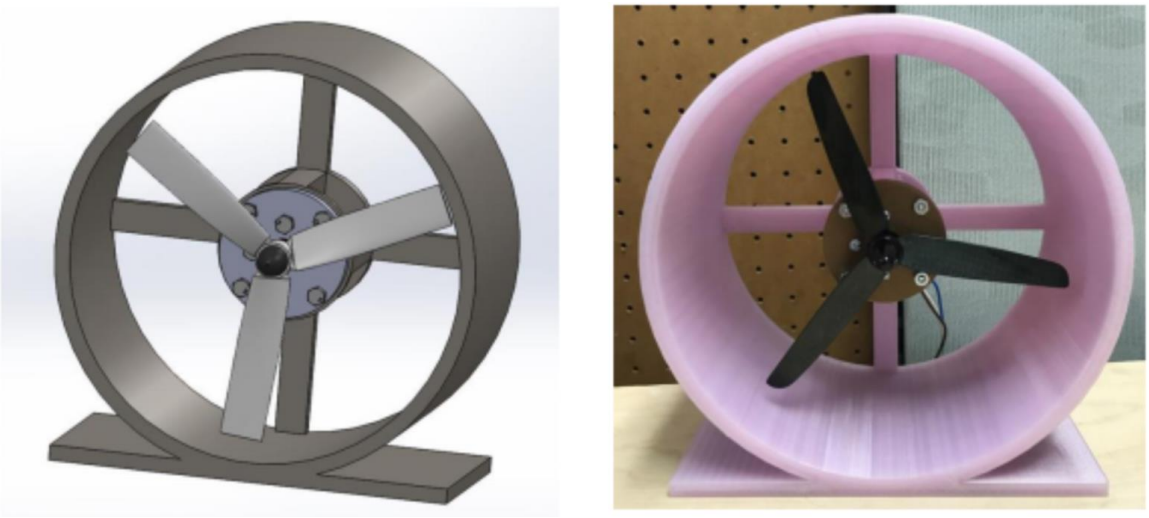

Figure 60- Cowling concept for wind turbine

Setup and cases compared

The setup and boundary conditions for this analyses was the same as the previous analysis from section 5.1.2.1 Convergence check and comparison to BEM results shown in Figure 55. However, an additional geomtry was added as shown in the cases 1-5 shown below; geometries added are shwon in Figure 61-Figure 65.

Case 1: Blade only

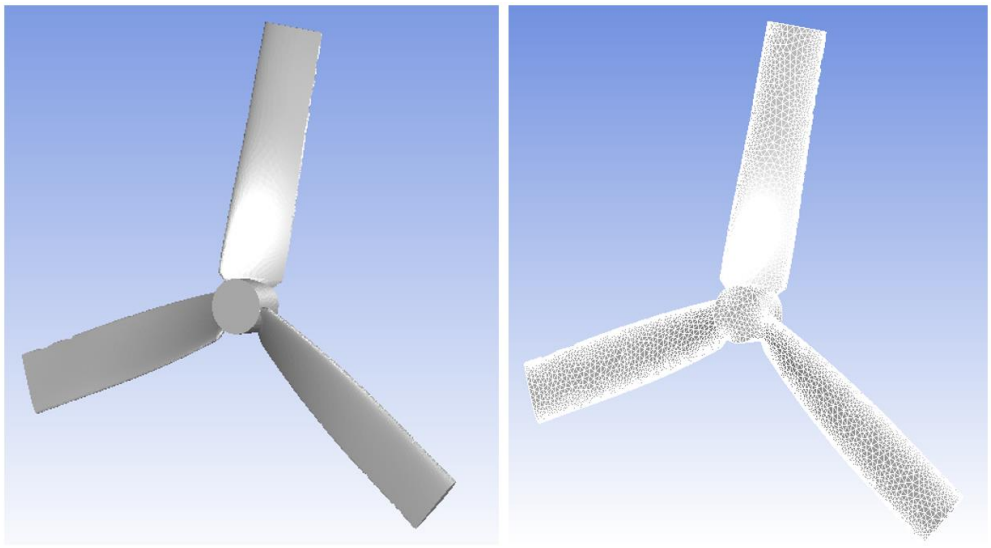

Figure 61-CFD analysis of blade case 1 geometry and mesh

Case 2: Blade and generator

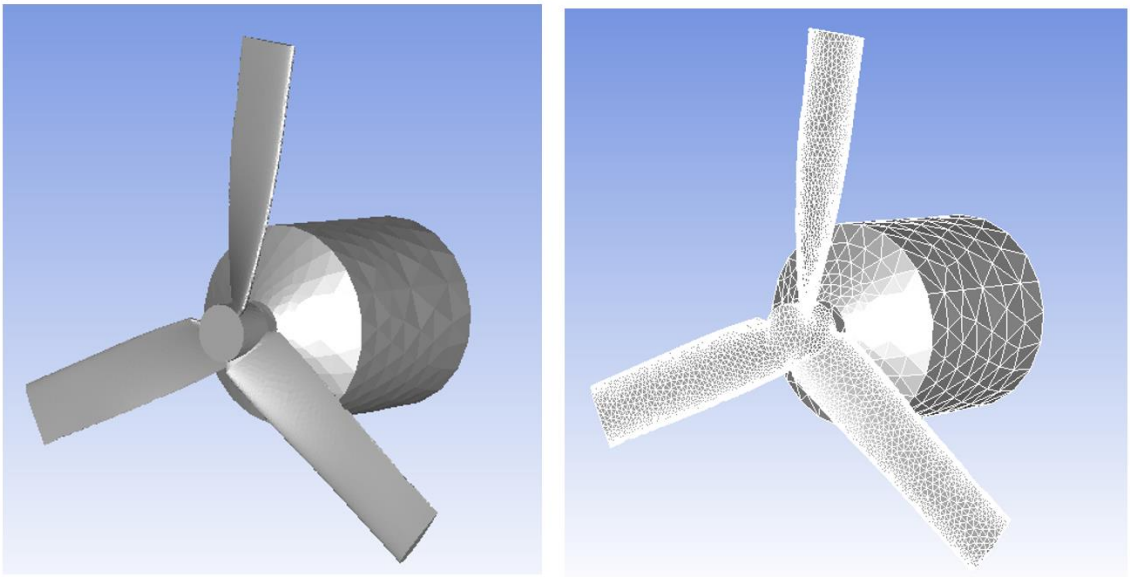

Figure 62-CFD analysis of blade case 2 geometry and mesh

Case 3: Blade with generator and **7 inch inner diameter cowling,** ¼ in wall thickness and ½ in supports

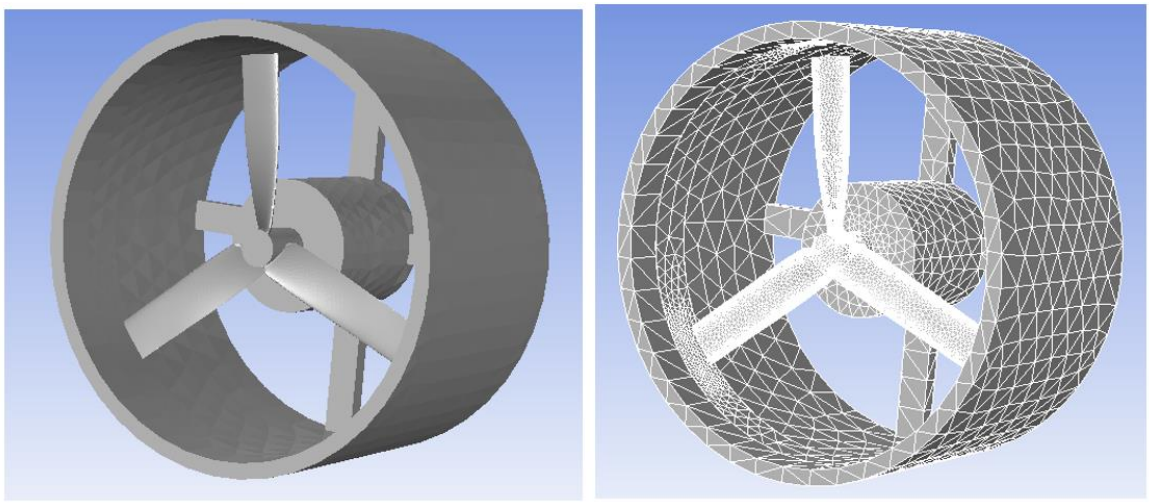

Figure 63-CFD analysis of blade case 3 geometry and mesh

Case 4: Blade, generator with cowling **8 inch inner diameter, thinner walls** (1/8 inch) and supports (1/4 inch)

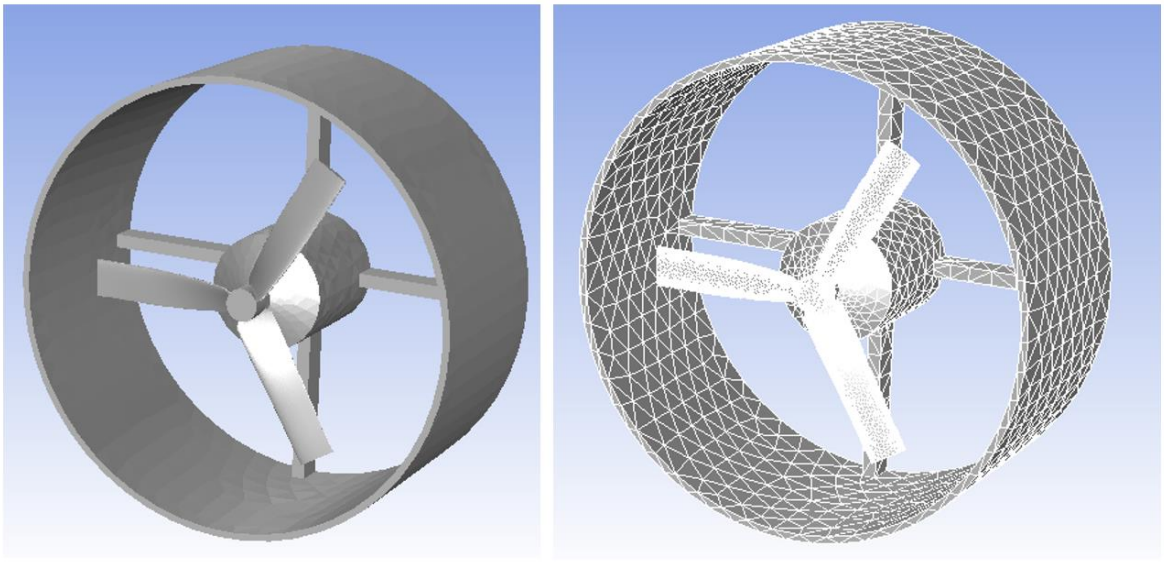

Figure 64-CFD analysis of blade case 4 geometry and mesh

Case 5: Same geometry as Case 4 but with slots (1/8 in walls, 1/4 inch supports and 8 inch inner diameter)

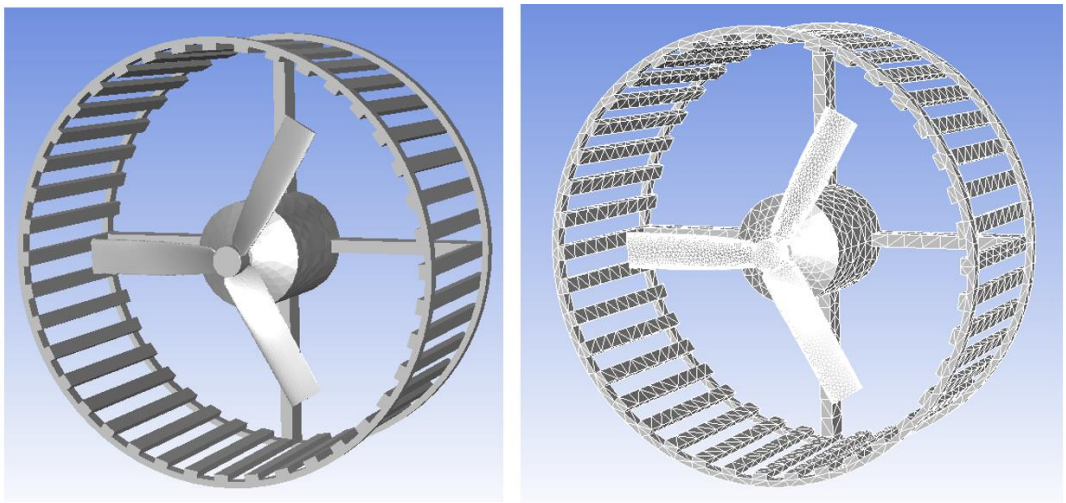

Figure 65-CFD analysis of blade case 6 geometry and mesh

Figure 66 and Figure 67 shows the torque and power curves for the CFD simulations. Changes on the cowling designs were made to check if the power loss could be reduced. The plots in Figure 66 and Figure 67, as well as Table 5 show that adding slots to the cowling would reduce the power loss as opposed to having the solid cowling.

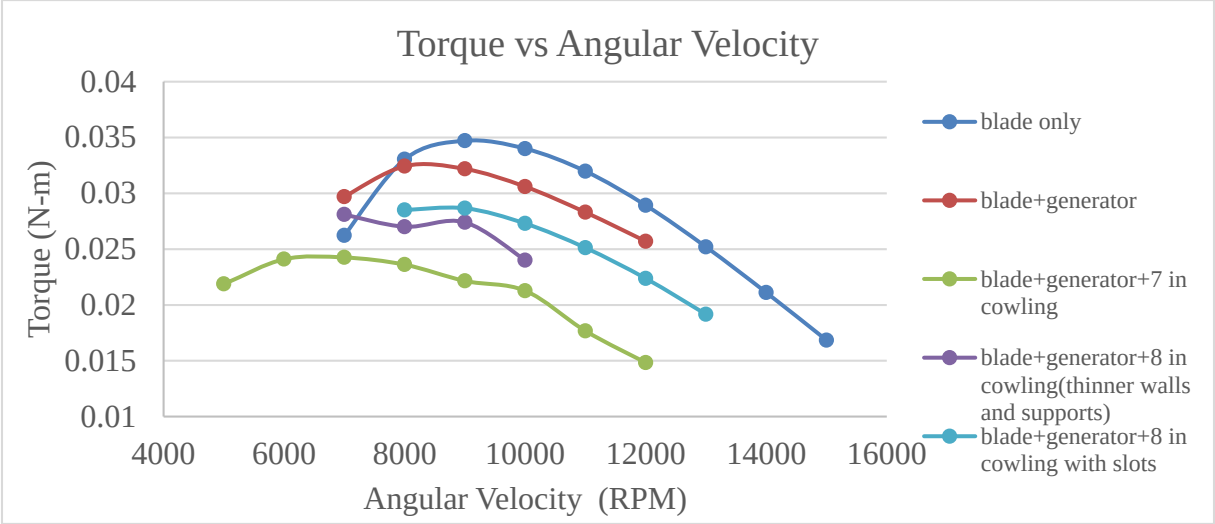

Figure 66-Torque curves for each of the CFD analysis cases

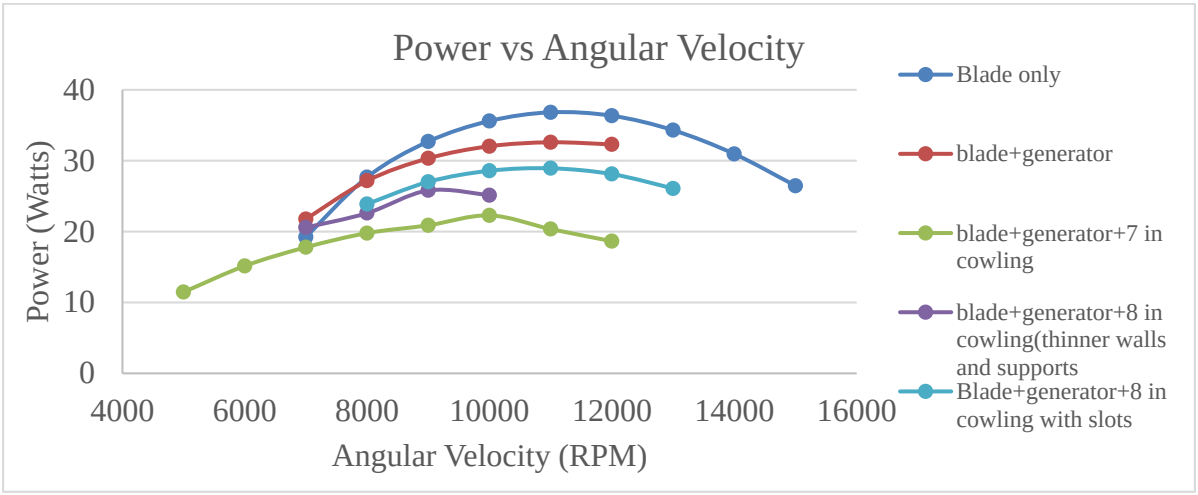

Figure 67-Power curves for each of the CFD analysis cases

Table 5 shows the maximum power result for each of the cases. It is important to note that the order of the runs was:

- Initially the blade by itself (Case 1)
- The blade was modeled with cowling and generator to check effects of adding a cowling (Case 3)
- The cowling was made thinner in its walls and supports, the diameter was increased from7 to 8 inches (Case 4)

- After seeing that the larger diameter, thinner cowling improved the power performance of the blade, the blade was left with only the generator to check the effect of the generator on power. (Case 2)
- Next, slots were added to the 8 in, thinner cowling (Case 5)

Table 5-Maximum power results for each CFD analysis case

Case #	**Description**	**Max Power (Watts)**
1	6 inch Blade only	36.8
2	Blade with generator	32.6
3	Blade, generator & 7 in cowling	22.3
4	Blade, generator & 8 in cowling (thinner)	25.8
5	Blade, generator & 8 in cowling with slots	28.9

Table 5 shows the power loss caused by adding generator or cowling in different configurations, summary below:

- Adding a generator decreases the max power of the 6 inch blade by 11.4% (36.8 to 32.6 watts); a longer shaft should make the drop lower
- Adding 7 in cowling+generator decreases blade max power by 39.4% (36.8 to 22.3 watts)
- Adding a 8 in cowling(thinner)+generator decreases blade max power by 29.9% (36.8 to 25.8 watts)
- Adding a 8 in cowling with slots+generator decreases blade max power by 21.5% (36.8 to 28.9 watts).

5.2 Mecaflux Heliciel (blade optimization software)

Mecaflux Heliciel is a software that assists in the design of wind turbine blades given inputs. As discussed in Section 2 for Aerodynamics of wind turbines, the chord length and/or twist angle can be manipulated at each of blade elements to maximize power output.

The inputs for Mecaflux Heliciel are: wind velocity and density, blade and hub diameter, number of elements or profiles, chord length distribution, airfoil and airfoil maximum thickness as previously defined in Figure 5; the software then gives the option inputting angular velocity or calculating the optimal angular velocity for the given parameters or inputs.

From the inputs, the software then calculates the optimal twist angles for each element using the BEM method along with maximum power output. Another good feature the software has is making analysis for a blade at multiple angular velocities, which would then give torque vs angular velocity (or power vs angular velocity) curves.

There's an option to refresh twist for each blade element at each angular velocity for given inputs, or to maintain the same twist. For this analysis, the twist for each element was refreshed at each angular velocity.

5.2.1 Design of optimal blade twist

The design inputs used are: 50 mph wind velocity, 7 in diameter, .7 in hub diameter, 6 profiles or 5 blade elements. Several chord lengths distributions were used throughout the analysis; however, it was found that a constant chord length usually provided better results. Also, the maximum thickness was varied for the generation of torque and power curves.

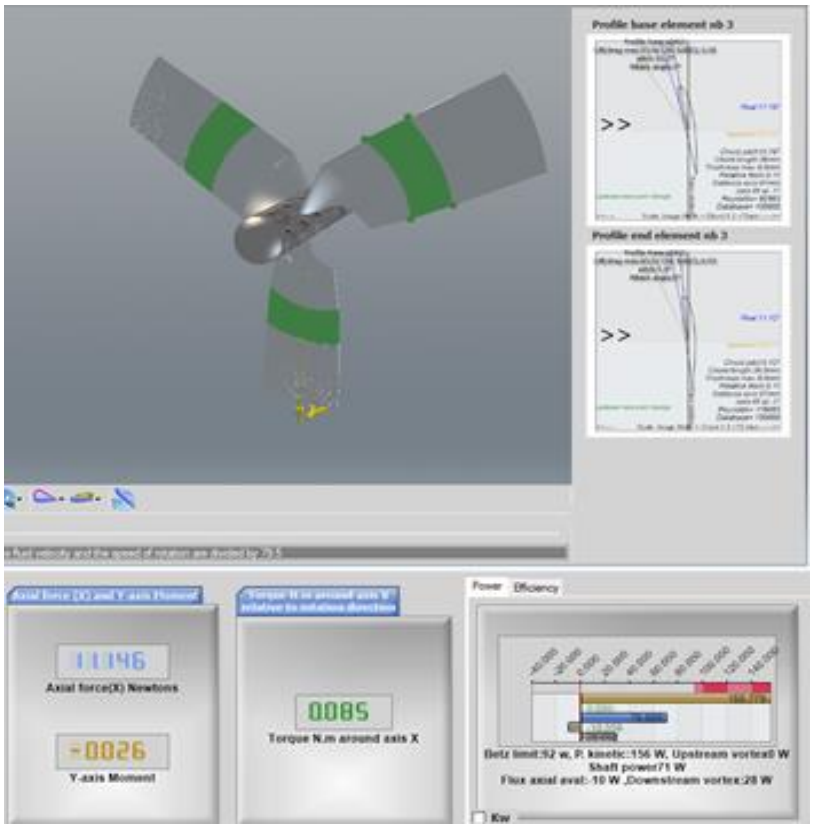

Figure 68-Sample design specification output from Mecaflux Heliciel software

Figure 68 shows the user interface for Mecaflux Heliciel software showing sample axial force, moment and torque results for a wind turbine blade. Figure 69 shows the definitions for the outputs from Mecaflux Heliciel software.

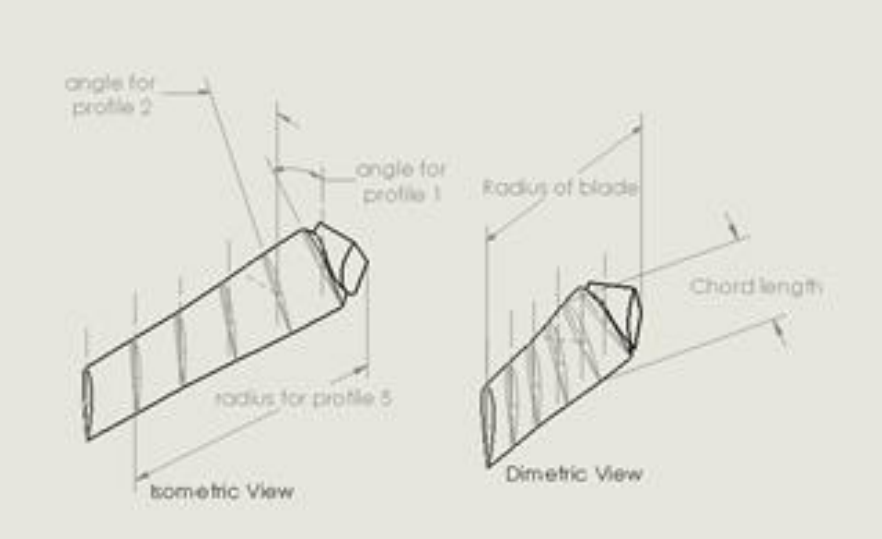

Figure 69-Definition of blade dimensions

5.2.2 Generation of power curves for blades

As mentioned previously, the Mecaflux Heliciel software has a function which permits creating blade power or torque curves. The software optimizes twist at each specified chord length and thickness of airfoil, to get maximum power. Several curves were created with chord length varying from 24-36 mm (0.9-1.4 in) as shown in Figure 70. This blade power curves would serve to correlate with electrical system power curves and then the maximum point of intersection would serve as the point of design for the optimal blade design to transfer most power to battery.

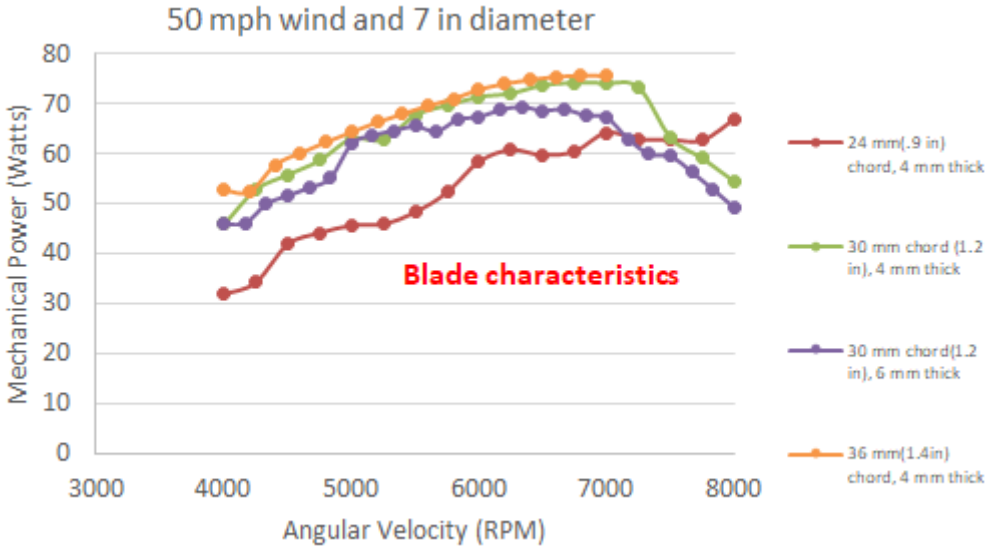

Figure 70-Wind turbine blade characteristic power curves

5.3 Choice of optimal blade design

In this section, an optimal blade design that produces maximum power transfer through the electrical system is chosen, the dimensions obtained from Mecaflux Heliciel are described and drawn into Solidworks. Next, a stress Finite Element Analysis (FEA) is performed on the blade at maximum expected angular velocity of 10,000 RPM to make sure the blade won't fail; factor of safety was found to be 3.4.

5.3.1 Experimental electrical and theoretical blade curves correlation

The previously obtained electrical system curves for different State of Charges of 80-100% were overlapped for the blade curves for constant chord lengths of 24-35 mm. Correlation of blade and electrical system curves are shown in Figure 71. The correlation shows that the highest point of intersection occurs between the 80% SOC curve and 36 mm(1.4 in) chord length blade; and corresponds to an angular velocity of 6300 and would yield power of 75 Watts (or 45% efficiency).

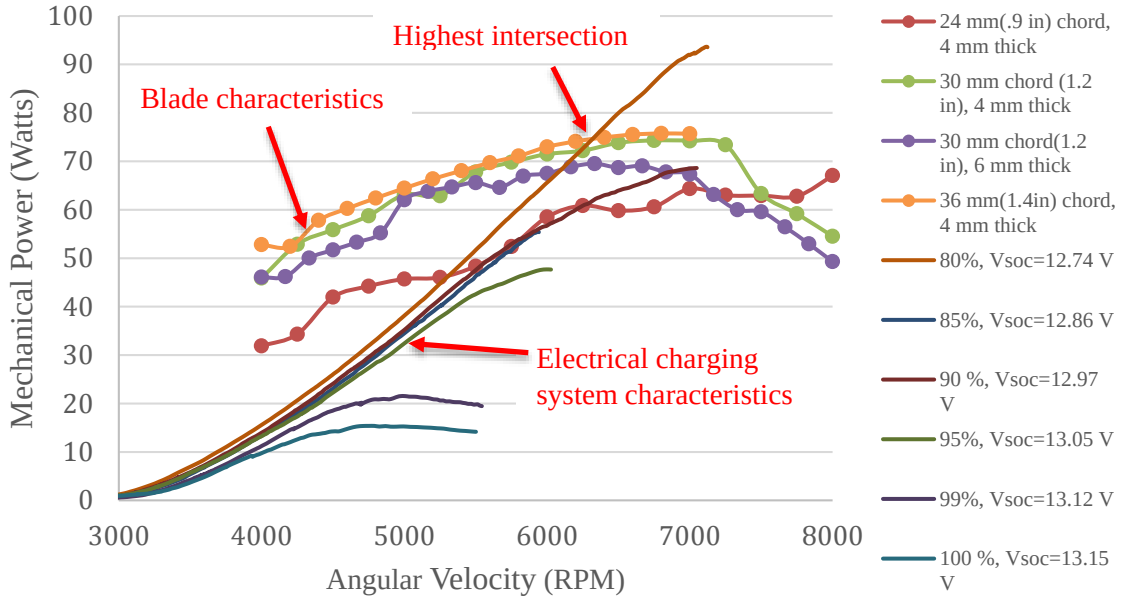

Figure 71-Correlation of experimental electrical system power curves and theoretical blade power curves

5.3.2 CAD and specifications of optimal blade

The design specification for the highest point of intersection was than obtained from Mecaflux Heliciel software. The blade has a constant chord length of 1.42 inches a hub diameter of .47 in, outer hub diameter of 3.5 in, and the airfoil used across all elements is NACA 2411. Table 2 shows the dimensions for the blade.

Table 6- Optimal Blade dimensions (for airfoil: NACA 2411)

	Radius r (in)	Twist Angle θ p (degrees)	Chord length c (in)	Thickness (in)
profile 1	0.47	62.47	1.42	0.16
profile 2	1.08	27.47	1.42	0.16
profile 3	1.68	18.61	1.42	0.16
profile 4	2.29	10.59	1.42	0.16
profile 5	2.89	5.97	1.42	0.16
profile 6	3.50	1.39	1.42	0.16

Figure 72 shows a section of optimal blade was than drawn in Solidworks following measurements from Table 6 showing the location of the twist angles to illustrate where the profiles are. Figure 73 shows the final blade design isometric view in Solidworks. It is important to note that the blade hub was designed so that it could be assembled to the generator. Also, stress analyses were performed on the blade designed as described in Section 5.4 to make sure the blade had a high factor of safety when operating at expected conditions

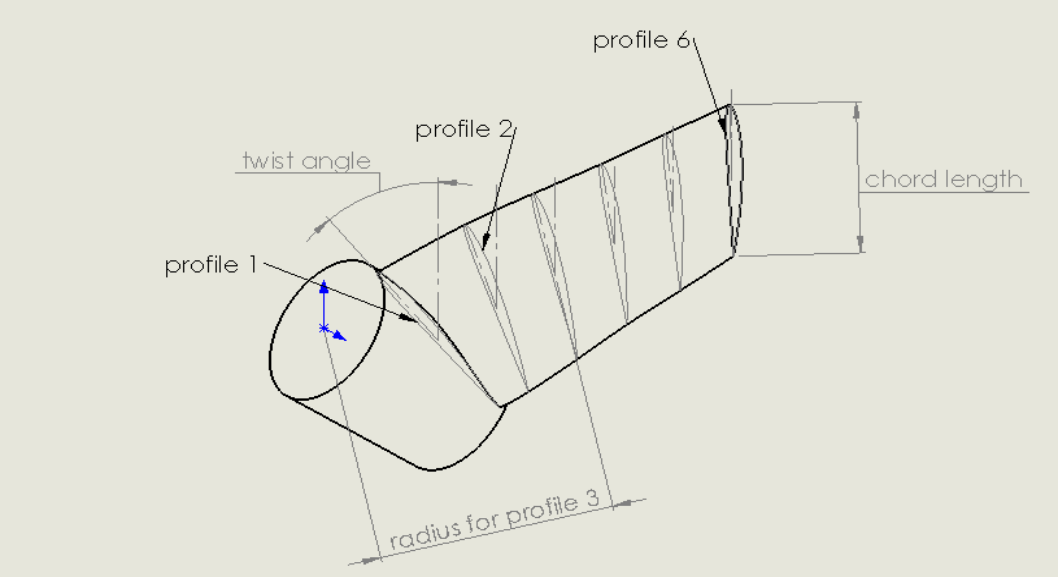

Figure 72-Sketch of optimal blade showing blade dimensions

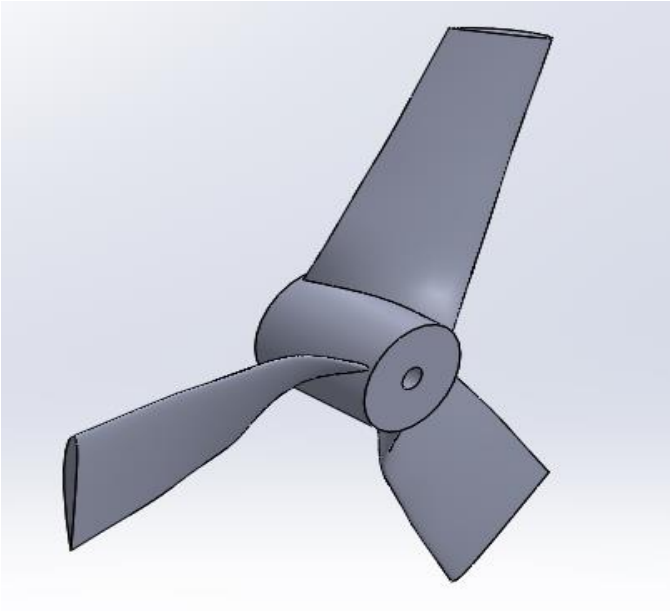

Figure 73-Isometric view of optimal blade

5.4 Stress finite element analysis

After coming up with the optimal design of the wind turbine blade, a stress finite element finite element analysis was done to confirm its integrity at expected operating conditions. The model was imported to ANSYS and meshed to about 13,000 elements.

The material properties applied to the model were those for VeroWhite Plus 3d printing material with ρ=1170 kg/m^3, E=2500 MPa, Poisson's ratio was assumed to be v=0.3, and UTS=58 MPa. The boundary conditions applied to this model were: a cylindrical support at inner diameter of hub and a maximum angular velocity of 10,000 RPM (or 1047 rad/s) for maximum power.

Figure 74 show Von Mises stress contour plot of the entire blade while Figure 75 shows a zoomed in view of the area close to the hub which had the highest stresses. Figure 76 shows a factor of safety contour plot, factor of safety being defined as the ultimate tensile strength divided by max Von Mises stress. Factor of safety is shown to be 3.4

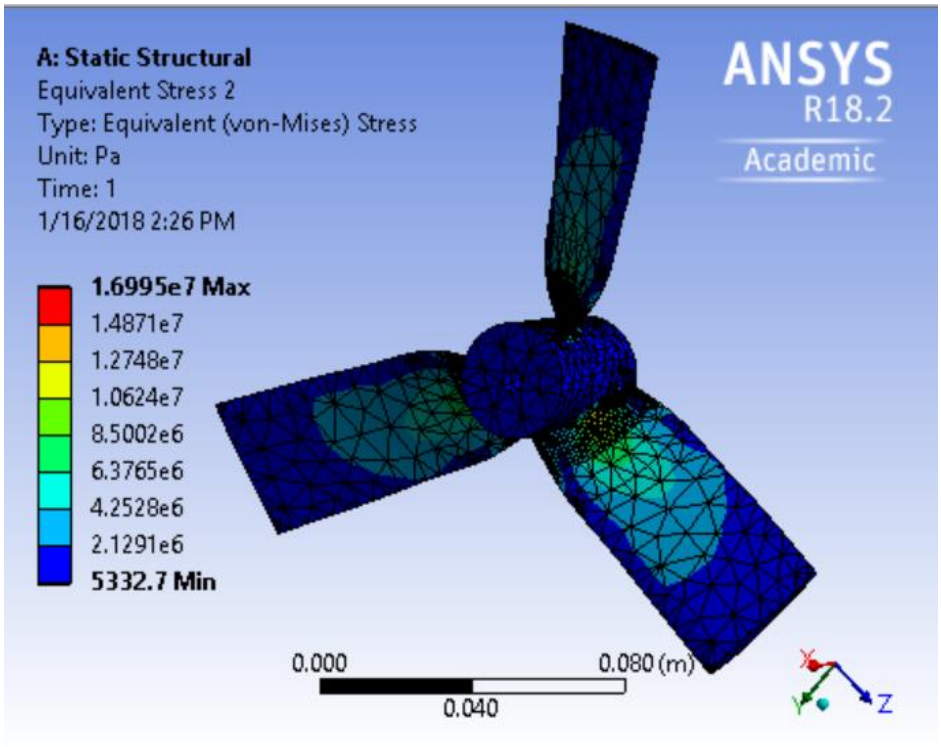

Figure 74-Wind turbine blade Von Mises stress results

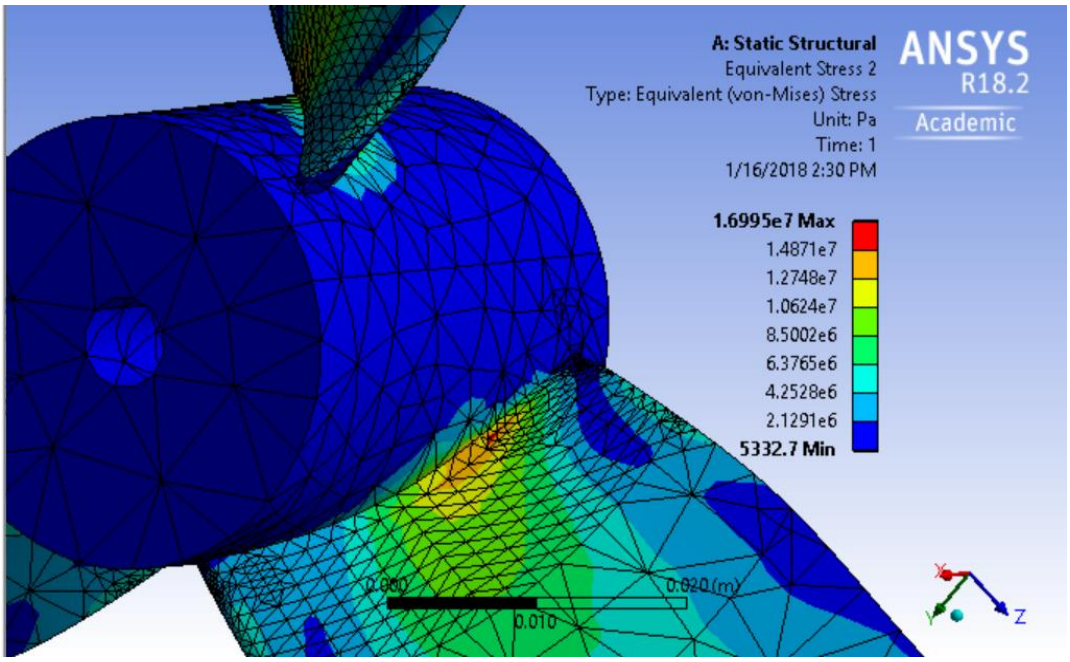

Figure 75-Wind turbine blade Von Mises stress results zoomed in

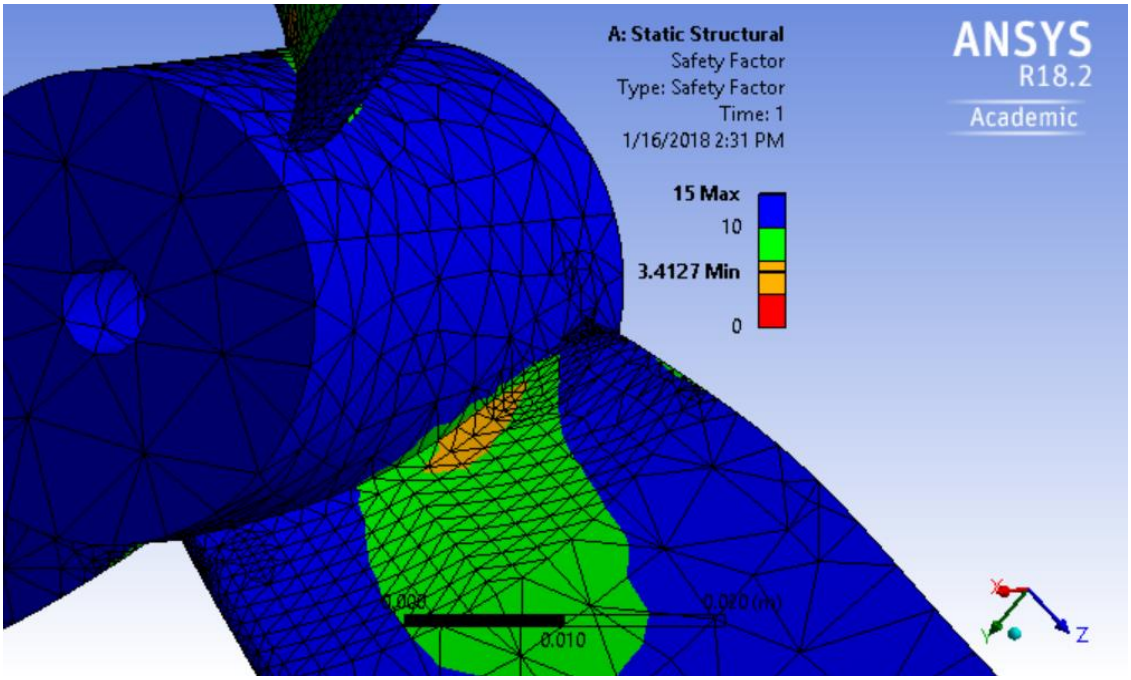

Figure 76-Wind turbine blade factor of safety results zoomed in

Figure 76 shows that the minimum safety factor is 3.4 and is located close to where the blade connects with the hub. Therefore, the blade is safe to operate at the expected maximum angular velocity of 10,000 RPM.

5.5 Qblade (blade analysis software)

Qblade is a simulation software for wind turbine blade design and aerodynamic simulation. Like Mecaflux Heliciel software, it uses Blade Element Momentum (BEM) theory to solve for the forces in a wind turbine blade given blade element dimensions. In this work, Qblade is used to compare results from previously obtained results in Mecaflux Heliciel; results are shown in Chapter 6.

6. WIND TURBINE TESTING AND EXPERIMENTAL VALIDATION

6.1 Torque, power and efficiency curves generation for wind turbine blade

The optimized 7 in blade was setup as shown in Figure 77. In this test, the wind turbine is placed in front of the wind tunnel. The wind turbine blade is then connected to a generator, which is mounted to the Interface reaction torque transducer. The generator is connected to a resistor bank; where the resistance is varied in order to control the angular velocity of the system. Bumper bearings (or bearing with a clearance to the shaft of .0125 in were added) were added as shown in Figure 77 to protect torque sensor and generator in case of a blade failure. However, due to the flexibility of the 3d printed parts, the shaft could touch the bumper bearings when vibrating; therefore, the bearings were removed and system was tested at a lower wind speed.

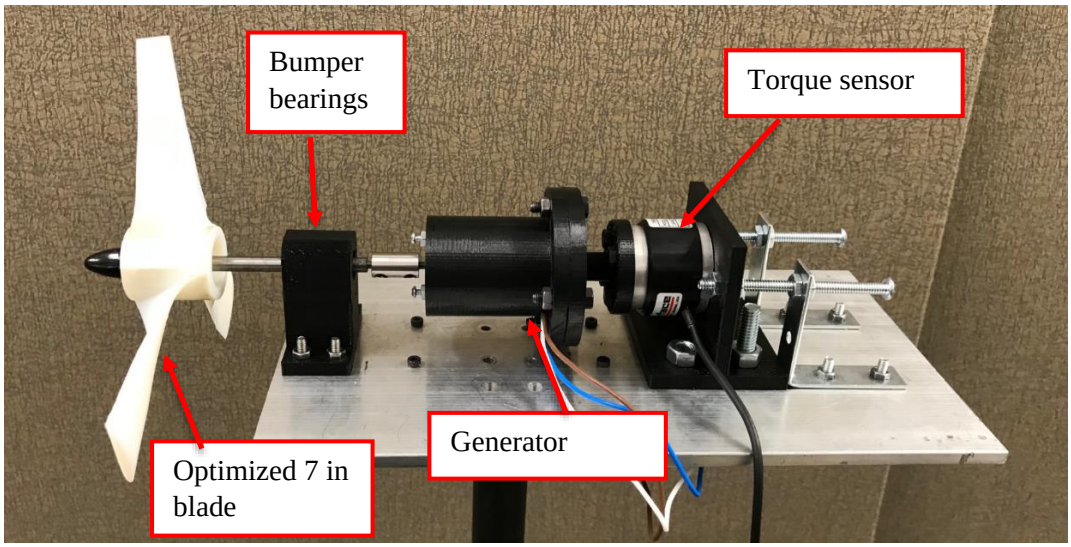

Figure 77-Assembled wind turbine test fixture with reaction (non-rotating) torque transducer

Due to the high vibrations at angular velocities higher than 5000 RPM, the system was initially tested at a wind speed of 20 mph and the angular velocity was checked to be below 4000 RPM. However, later on the vibration problems were fixed by adding a bearing in press fit with the shaft and the system was tested at 50 mph and up to 10,000 RPM angular velocity. The press fit bearing wasn't added previously because it would cause a power loss.

First, the torque, power and efficiency results and correlation for the system at 20 mph is presented. Next, the correlation of theoretical and experimental results for the 50 mph wind test are presented.

20 mph torque, power and efficiency experimental results

Figure 78-Figure 80 show the torque, power and efficiency experimental curves for the test done on the 7 inch blade. The efficiency curve shows that the blade reaches an efficiency of 45% when rotating at around 3,300 RPM; this is a good efficiency considering that commercial wind turbines have an efficiency of close to 40-45% (Betz limit or maximum theoretical efficiency, Cp= 59%). The next step is to correlate to theoretical data obtained from Mecaflux Heliciel and Qblade Blade Element Momentum (BEM) software's.

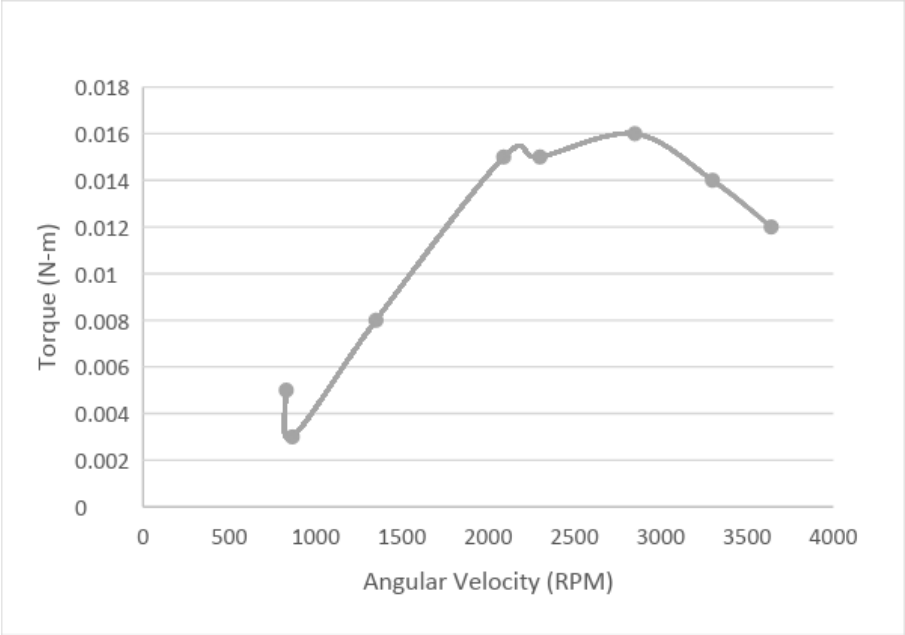

Figure 78-Experimental torque curve for optimized 7 in blade at 20 mph wind

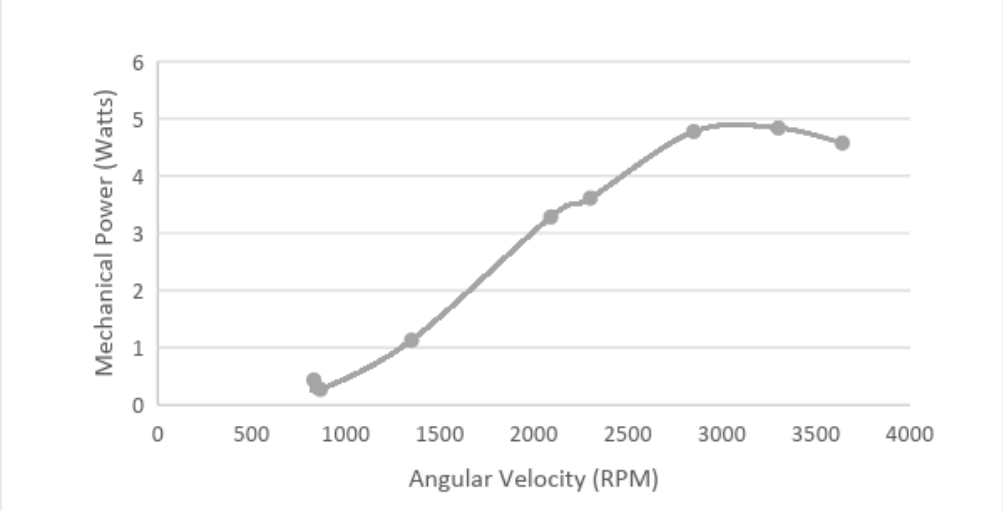

Figure 79-Experimental mechanical power curve for optimized 7 in blade at 20 mph wind

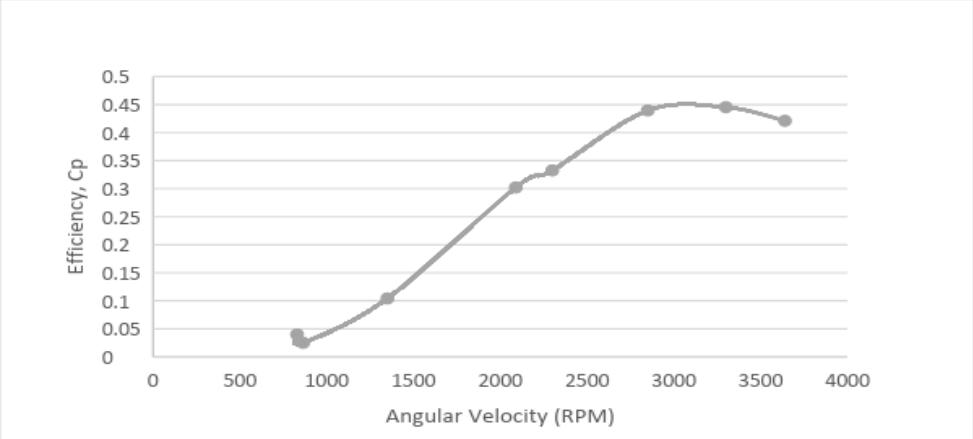

Figure 80-Experimental efficiency curve for optimized 7 in blade at 20 mph wind

6.2 Test-theory correlation on blade torque vs RPM

20 mph torque, power and efficiency experimental and theory correlation

Next, experimental curves obtained in the testing at 20 mph and angular velocity range of 800-3600 RPM are correlated with previously obtained theoretical data from Mecaflux Heliciel software. Also, new theoretical data from Qblade software is added to the plots. Figure 81-Figure 83 show torque, power and efficiency curve correlation between experimental and theoretical data.

Figure 81 shows that the experimental torque data falls between the theoretical torque results from Blade Element Momentum software's Mecaflux Heliciel and Qblade. The maximum torque of 0.025 N-m from Qblade software is significantly higher than the maximum torque of 0.016 N-m from the experiment. However, it is more important to compare power and efficiency curves.

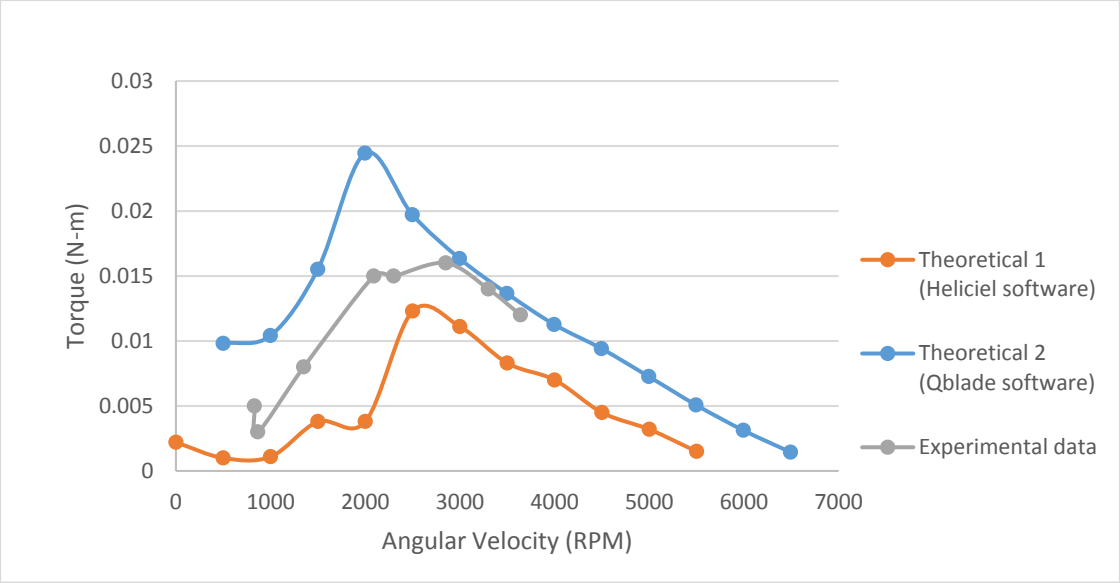

Figure 81-Experimental and theoretical comparison of torque curve for optimized 7 in blade at 20 mph wind

The power curves in Figure 82 are obtained by multiplying the measured torque at its respective angular velocity. The maximum power for the experiment was found to be 4.8 watts at an angular velocity of 3,300 RPM. While the maximum power for the theoretical results were found to be: 3.5 Watts at 3000 RPM for Heliciel software, and 5.2 Watts at 2500 RPM for the Qblade software. The maximum experimental power compares better with the theoretical results from Qblade software and is within 4% difference.

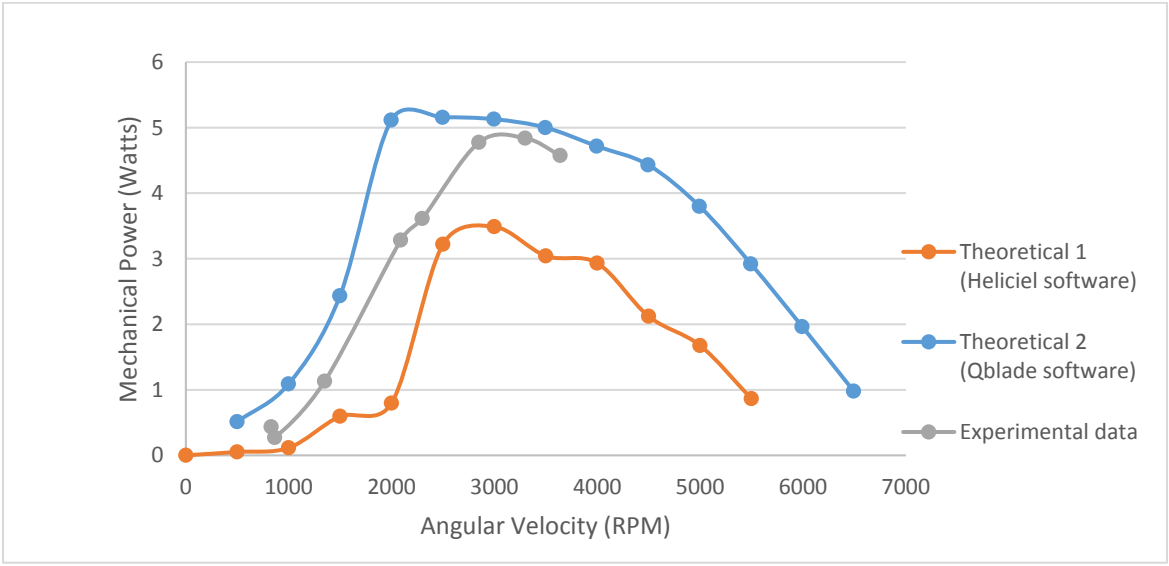

Figure 82-Experimental and theoretical comparison of power curve for optimized 7 in blade at 20 mph wind

The efficiency curves in Figure 83 have the same shape as the power curves in Figure 82; the maximum efficiency of 45% occurs at an angular velocity of 3300 RPM for the experimental case. The maximum theoretical efficiency from Heliciel software of 32% occurs at an angular velocity of 3000 RPM; while the maximum theoretical efficiency from Qblade software of 47% occurs at 2000-3000 RPM range. The maximum experimental efficiency correlates better with the theoretical results from Qblade software and is within 4% difference.

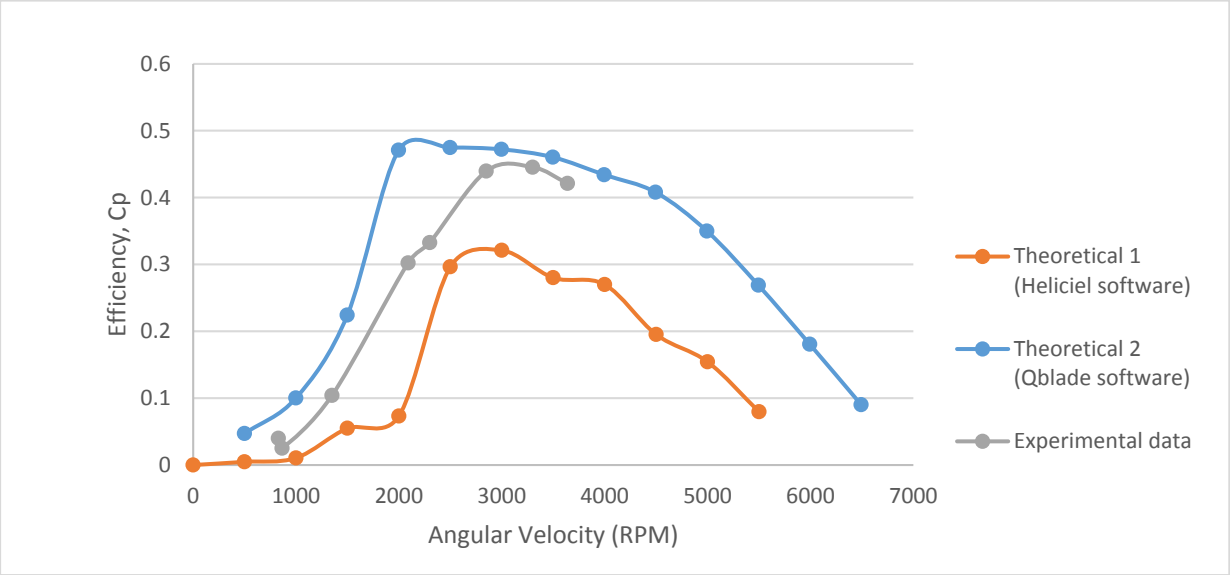

Figure 83-Experimental and theoretical comparison of efficiency curve for optimized 7 in blade at 20 mph wind

50 mph torque, power and efficiency experimental and theory correlation

Torque, power and efficiency correlations between experimental and theory at a 50 mph wind are shown in Figure 84-Figure 86. Experimental results were obtained for an angular velocity range of 9,600-10,300 RPM. As previously mentioned, the angular velocity was controlled by modifying the resistors connected to the generator leads. The lowest resistance produced an angular velocity of 9,600 RPM. Future work includes modifying the setup to be able to go below 9,600 RPM and get results for a larger angular velocity range.

In this case, the power is lower than predicted in the theoretical results. The press fit bearing that protects the generator and torque sensor from radial loads might be the cause of the power loss. The maximum power obtained at 50 mph was found to be 60 Watts which corresponds to an efficiency of about 35%. Theoretical efficiency at this operating range is close to 40% and 45%

for Heliciel and Qblade software respectively. The 5-10% loss of efficiency (or 10-15 Watts power loss) might be due to the bearing in press fit.

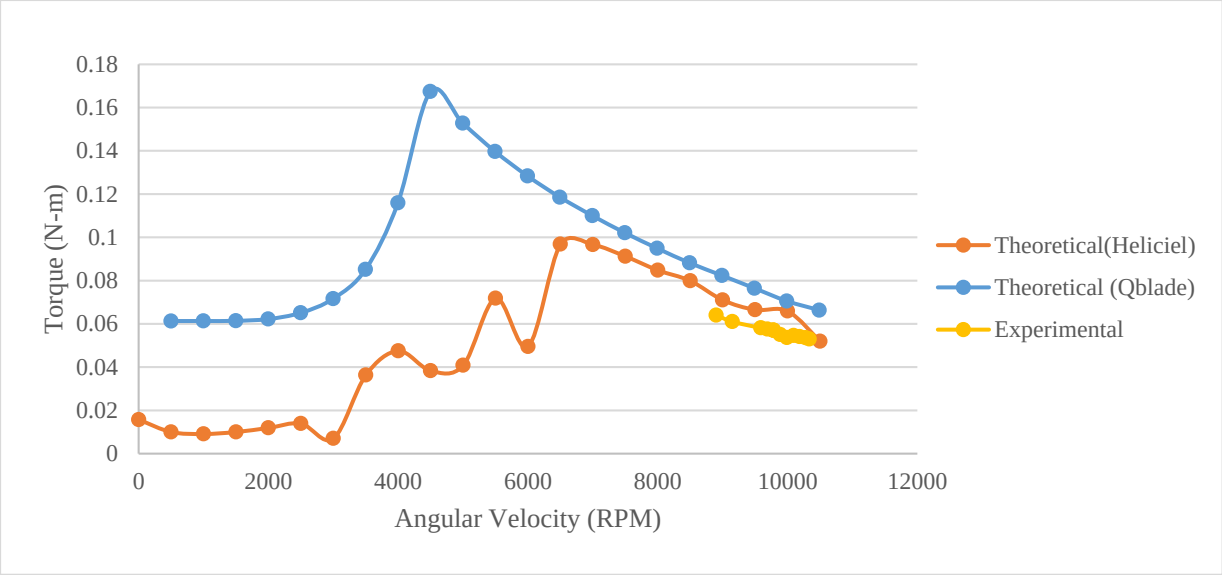

Figure 84-Experimental and theoretical comparison of torque curve for optimized 7 in blade at 50 mph wind

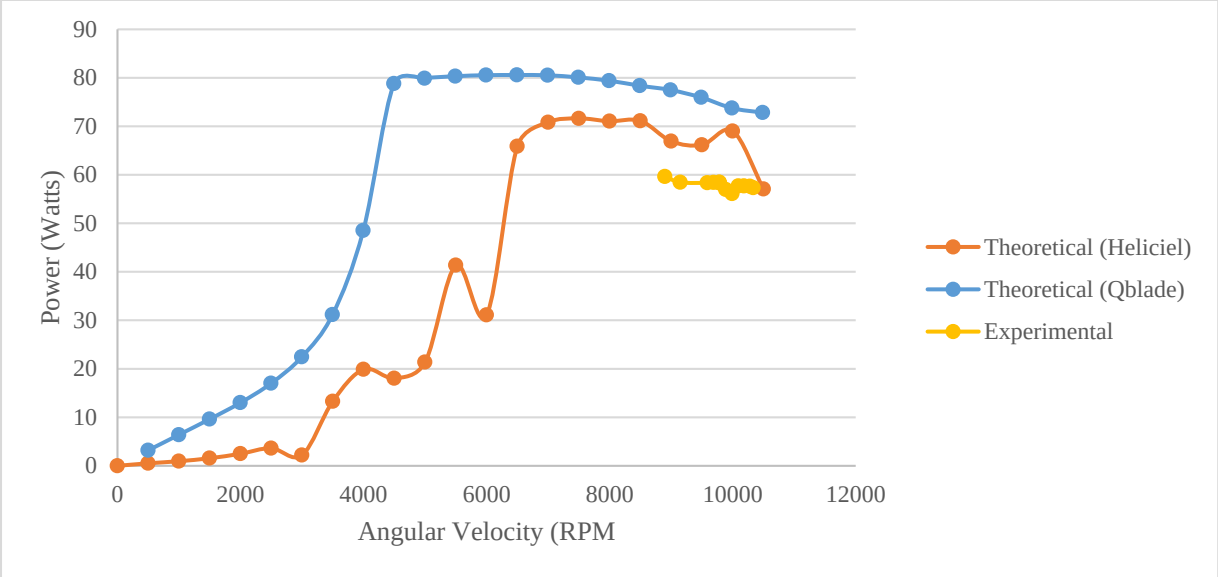

Figure 85-Experimental and theoretical comparison of power curve for optimized 7 in blade at 50 mph wind

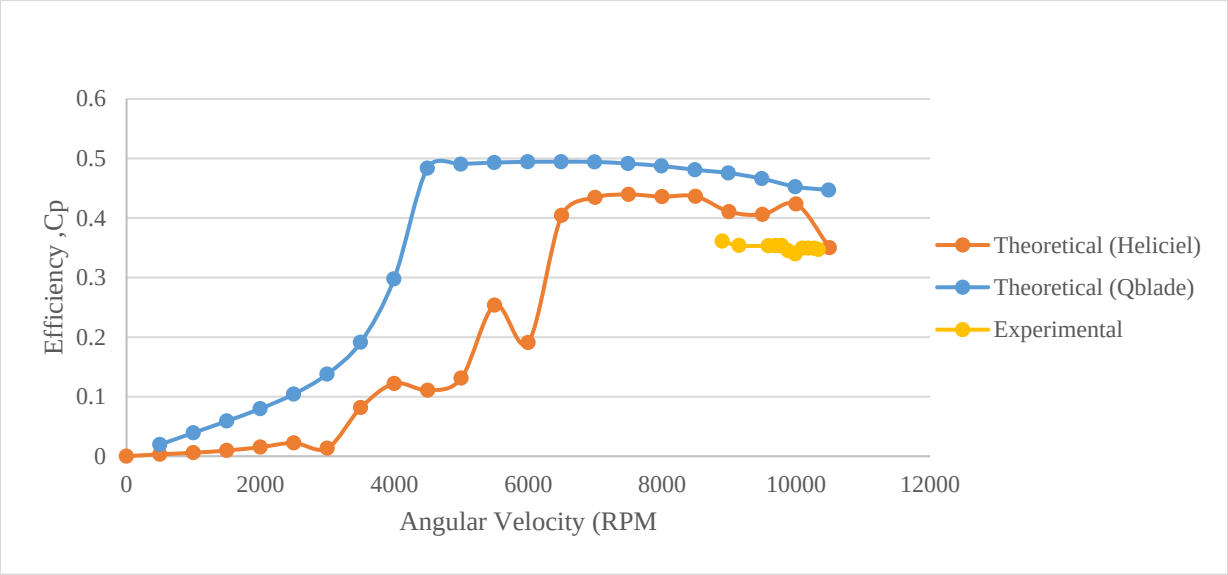

Figure 86-Experimental and theoretical comparison of efficiency curve for optimized 7 in blade at 50 mph wind

7. CONCLUSIONS AND FUTURE WORK

The main objective of this work was to optimize a wind turbine blade that would be used to harvest energy from the wind going against train movement; develop a charging system for a lead acid battery; manufacture blades and charging system; and test the system at expected wind conditions in a wind tunnel. A 7 inch diameter for the wind turbine blade was chosen taking into account: typical wind turbines have an efficiency of 40-45%; electrical system efficiencies; and expected 50 mph wind velocity.

A blade was designed taking into account charging electrical system power requirements. Characteristic torque and power curves were obtained for battery SOC's of 85-100% and blade chord lengths (or widths) of 24-36mm (.9-1.4 inch). Maximum power intersection between blade and electrical system characteristic curves was chosen as point of design for wind turbine blade

The blade's chord length and twist angle distributions were optimized by using Blade Element Momentum (BEM) software Mecaflux Heliciel. The optimized blade was structurally analyzed using ANSYS Structural for which a factor of safety of 3.4 was calculated at maximum expected operating conditions. Next, the blade was manufactured using a 3d printer and tested in a test rig.

Due to system high vibrations at high expected optimal rotational speed of 7,000 RPM at assumed 50 mph wind; experimental torque, power and efficiency curves were obtained through testing of wind turbine blade instead at a 20 mph wind and between 800-3600 RPM. Maximum efficiency and power between experimental and theoretical results were found to be within 4% difference. Efficiency of optimized wind turbine blade was found to be 43% which is very close to typical 40-45% efficiency of commercial wind turbines.

Preliminary testing was performed on optimized 7 inch blade when perceiving at 50 mph wind after fixing vibration problems of the wind turbine test fixture. Experiment results were obtained at a small angular velocity range of 8,900-10,300 RPM. Maximum experimental power was 60 Watts while theoretical ranged from 70-75 Watts for the same angular velocity range; percent difference between experimental and theoretical was within 13-20%.

Future work includes:

- Test and obtain experimental torque, power and efficiency curves for optimized 7 inch wind turbine blade at 50 mph wind; obtain full results (0-10,000) RPM.
- Test optimized 7 inch wind turbine blade at 50 mph wind to charge battery; compare SOC (State of Charge) vs time plots of nonoptimized and optimized blade.
- Investigate and develop wireless charging of batteries that are located in cars were there aren't wind turbines.

REFERENCES

[1] Manwell, J. F., McGowan, J. G., & Rogers, A. L. (2011). *Wind energy explained: theory, design and application*. Chichester: John Wiley & Sons.

[2] Burton, T. (2009). *Wind energy: Handbook*. Chichester: Wiley.

[3] García-Sanz, M., & Houpis, C. H. (2012). *Wind energy systems: control engineering design.* Boca Raton, FL: CRC Press.

[4] McCosker, J. (2012). *Design and Optimization of a Small Wind Turbine (master's thesis).* Rensselaer Polytechnic Institute.

[5] Gundtoft, S. (2009). *Wind Turbines*. Aarhus University

[6] Mecaflux Heliciel [computer software]. (2018). Retrieved from https://www.mecaflux.com/suite/en/heliciel.php

[7] QBlade-Wind Turbine Design and Simulation [computer software]. (2018). Retrieved from http://q-blade.org/

[8] Propeller calculation method used by the software heliciel. (n.d.). Retrieved February, 2018, from https://www.heliciel.com/en/logiciel-calcul-helice-aile/Methode-calcul-helice%20heliciel.htm

[9] Marten, D., Wendler, J., Pechlivanoglou, G., Nayeri, C. N., Paschereit C.O. (2013). *QBlade: An open source tool for design and simulation of horizontal and vertical axis wind turbines.* International Journal of Emerging Technology and Advanced Engineering, 3(3), 264-269. Retrieved February, 2018.